PETRA III Extension Project

Damping wiggler beamline P61
Large Volume Press instrument for extreme conditions (P61.2)

Technical Design Report

Review Version June 5, 2015

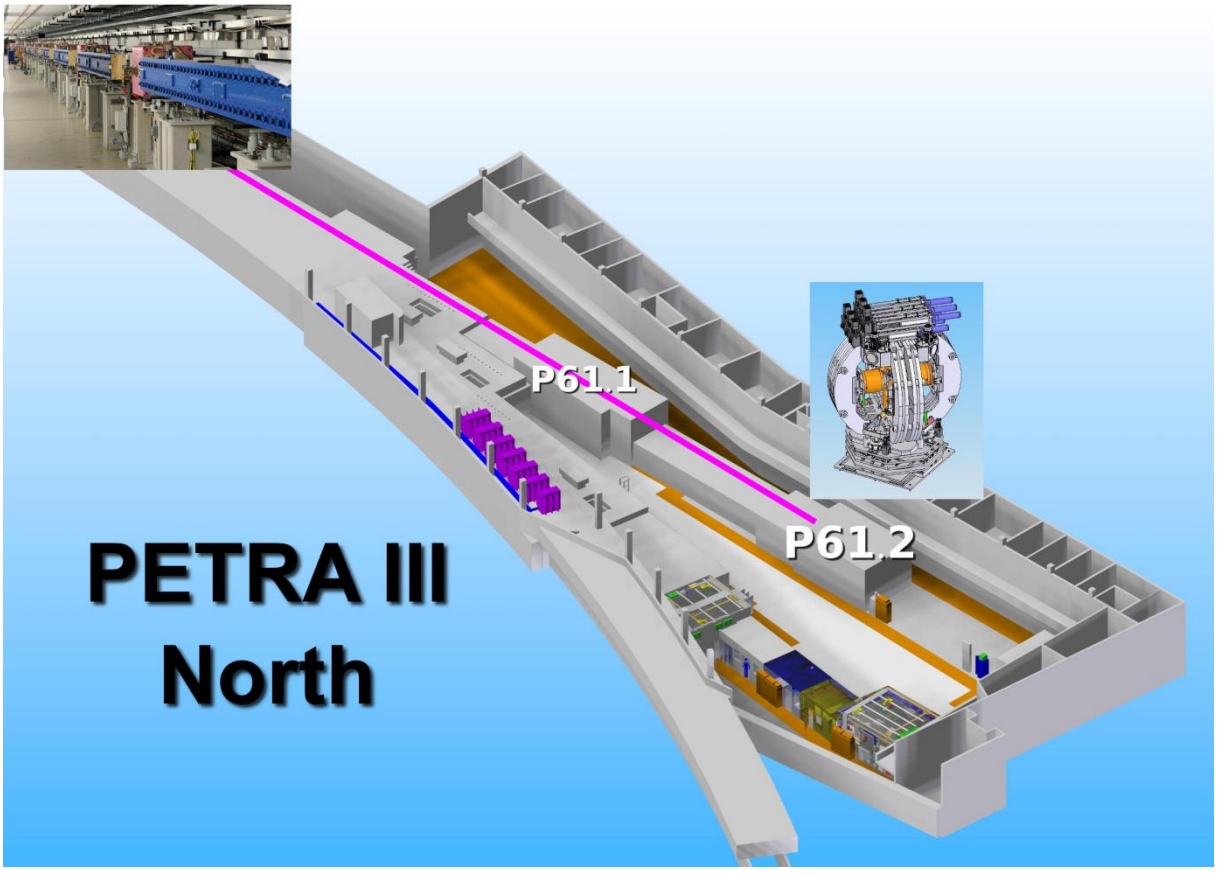

Contributors

DESY

Norimasa Nishiyama	Work package leader
Stefan Sonntag	Beamline engineer
Wolfgang Drube	Project leader PETRA III extension

Bavarian Geo-Institute Bayreuth

BMBF funded project (LVP-instrument)

Tomoo Katsura	Project leader

Contributing DESY groups

DESY Photon Science:

- FS-BT, beamline technology
- FS-TI, technical infrastructure
- FS-PEX, PETRA III Extension project

We acknowledge fruitful discussions with
H.-P. Liermann, U. Lienert and M. von Zimmermann.

Contents

1.	Introduction …….	1
1.1	PETRA III Extension ……..	1
1.2	Research of materials under extreme conditions at PETRA III …..……..	4
2.	Beamline and X-ray optics ……..…..	7
2.1	Layout and hutches ……..……..……	7
2.2	Damping wigglers …….....	10
2.3	Front end ……..……...	13
2.4	Optics hutch …….....	16
2.5	Experimental hutch …….....	17
3.	LVP instrument for P61.2 ……...…	19
3.1	Overview ……..……...	19
3.2	6-rams LVP instrument …….....	21
3.3	LVP stage ……...	24
3.4	Power supply for heating ……..…….	26
3.5	Compression geometry..……..…….	27
3.6	Attenuation of X-rays by high-pressure cells …….	34
3.7	Ex-situ LVP instrument.…….	37
3.8	Pressure cells for user experiments ..…….	37
4.	Detector and detector mount ……..……...…	39
4.1	Overview ……..……...…	39
4.2	Detector mount ……..……...…	40
4.3	Detector ……..……..…	43
4.4	Time-resolved energy dispersive X-ray diffraction measurements …..…	46
4.5	Stress analysis under high pressure and temperature ……..…	47
4.6	Liquid structure analysis using the 6-6 configuration ……..…..	48
5.	Future developments ……..……	50
5.1	High energy monochromatic X-ray capability ……..…	50
5.2	Multi-element SSD for stress analysis ……..…	55
5.3	Time-resolved high temperature XRD under 1 bar ……..……..…	56
	Time line ……..	58

1. Introduction

1.1 PETRA III extension

DESY is one of the world's leading accelerator centers and a member of the Helmholtz Association, Germany's largest scientific research organization comprising 18 scientific-technical and biological-medical research centers. It develops, builds and operates large particle accelerators used to investigate the structure of matter. Photon science is a major branch of its research activities and DESY has a long standing tradition in the use of synchrotron radiation. For almost 38 years, the 2nd generation facility DORIS served as a very productive high-flux source for synchrotron radiation based research until it was finally shut down in October 2012. Currently, the main photon sources at DESY are the storage ring PETRA III and the Free-Electron-Laser FLASH, offering unique research possibilities for an international scientific community.

PETRA III is a low-emittance (1 nmrad) 6 GeV storage ring having evolved from the conversion of the large PETRA accelerator into a 3rd generation light source. Construction started in 2007 and first beamlines became operational in 2009. Today, a total of 14 undulator beamlines are in user operation in the Max-von-Laue experimental hall covering 1/8 of the storage ring. The focus of this facility is on

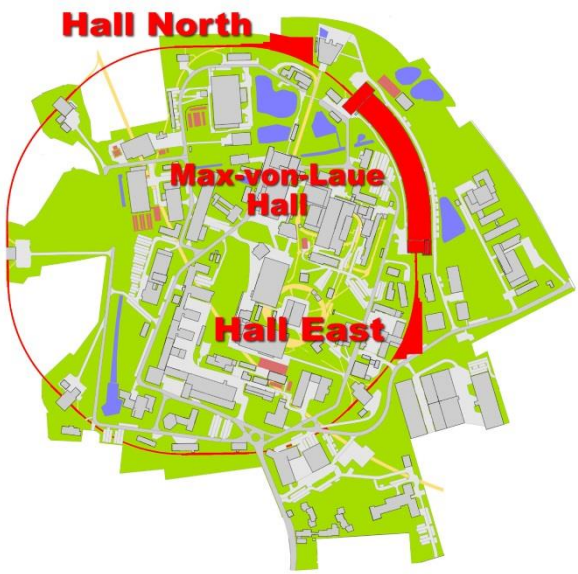

Fig. 1.1.1
View of the PETRA III storage ring (red line). The present experimental hall is shown together with the additional experimental halls in the North and East which are currently under construction.

applications making optimum use of the high beam brilliance especially at hard X-ray energies, i.e. experiments aiming at nano-focusing, ultra-high resolution studies and coherence applications. Because a number of very productive techniques formerly available at DORIS III are not currently implemented at PETRA III and the user demand for access to the new beamlines was anticipated to be very high, it was decided to extend the experimental facilities at the new source and to provide additional beamlines. This PETRA III extension project adds two new experimental halls on either side (North and East) of the current Max-von-Laue hall making use of the long straight sections and part of the adjacent arcs (see Fig. 1.1.1)

The northern straight section accommodates one of two 40 m long damping wiggler arrays producing an extremely hard and powerful x-ray beam which will be utilized for materials science experiments. This is the source of beamline P61 where the large volume press will be installed. The long straight section in the east is available for additional insertion devices. In order to accommodate insertion device sources in the arc sections, which are filled with long dipole magnets yielding a rather soft X-ray spectrum, the machine lattice will be modified. The new lattice adds double bent achromat (DBA) cells in the arcs, each allowing for a 5 m long straight section. Similar to the present PETRA III beamlines, these straights will serve two beamlines independently by use of canting dipoles resulting in two separate 2 m long straights. Different from the present 5 mrad canting scheme, a canting angle of 20 mrad was chosen at the extension beamlines to provide more spatial flexibility for the experiments further downstream. In total, the new lattice provides eight short straight sections in the two arcs with source properties corresponding to a high-beta section at PETRA III making them very suitable for the use of undulators.

Some of the new beamlines will be designed as ”short undulator” beamlines continuing most of the productive techniques formerly provided at DORIS III bending magnet beamlines. These sources will not only be very well suited for the spectrum of applications to be relocated from DORIS III but also provide a considerably brighter beam. In addition, high-brilliance long undulator beamlines will be built, three in collaboration with international partners Sweden, India and Russia. These beamlines will be located in hall east.

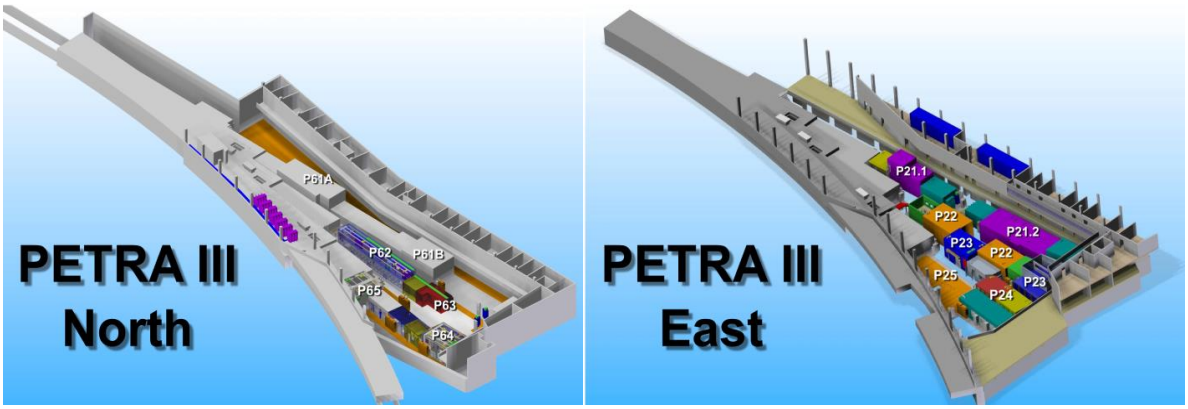

Fig. 1.1.2
Experimental halls PETRA III North (with beamlines P61 – P65) and PETRA III East (with beamlines P21 – P25).

Since 2009, the science case and specifications of the techniques to be implemented are being discussed with the user community, scientific advisory bodies and international partners. A number of specific user workshops have been held. A critical issue was the timing of the construction of the extension project because its realization required a complete shutdown of the current PETRA III user facility for an extended period of time. Also, a prioritization scheme has been defined for a successive implementation of the new beamlines in three phases (see Table 1.1.1).

Phase 1	Beamlines P64, P65
Phase 2	Beamlines P21.1, P21.2, P22, P23, P24
Phase 3	Beamlines P61, P66
Not funded yet	Beamlines P25, P62, P63

Table 1.1.1: Development phases of the PETRA III extension.

Phase 1 beamlines P64/P65 (X-ray absorption spectroscopy) are planned to become operational in September 2015. The civil construction of the PETRA III extension started in February 2014 by completely removing the storage ring at the site of the new experimental halls and demolishing the old concrete ring tunnel. In mid-August, 2014, the new tunnel areas inside the buildings have been completed and re-installation of the modified storage ring began while completion of the buildings outside continued. The technical commissioning of the modified storage ring began in December 2014 and regular user operation user operation at the present beamlines in the Max-von-Laue hall resumed in April 2015. The completion of the new facilities PETRA III North and East continues in parallel. At the time of this writing, civil engineering of the new halls is almost completed (Figs. 1.1.3 – 1.1.4) and the installation of technical infrastructure is in full swing.

Fig. 1.1.3
PETRA hall North as of May 2015.

Fig. 1.1.4
View into experimental hall PETRA III North (beamlines P61 – P65). Beamline P61 and the location of the LVP instrument is indicated.

1.2 Research of materials under extreme conditions at PETRA III

The existing PETRA III beamline P02.2 (Extreme Conditions Beamline) provides instrumentation to study materials under extreme conditions, i.e. high-temperature, low-temperature, high-pressure. The main tools to perform experiments under high-pressure conditions are diamond anvil cells (DAC) (Fig. 1.2.1 and Fig. 1.2.2). This device is portable and anvils are made of single crystal diamonds, which are optically transparent. Thus, a DAC is suitable for measurements using synchrotron radiation under high pressure and are also being been used at PETRA III beamlines, such as P01 for X-ray Raman scattering under high-pressure. However, there is no capability yet of extreme condition research using a large volume press (LVP) at PETRA III.

Fig 1.2.1
View of a typical diamond anvil cell (DAC)

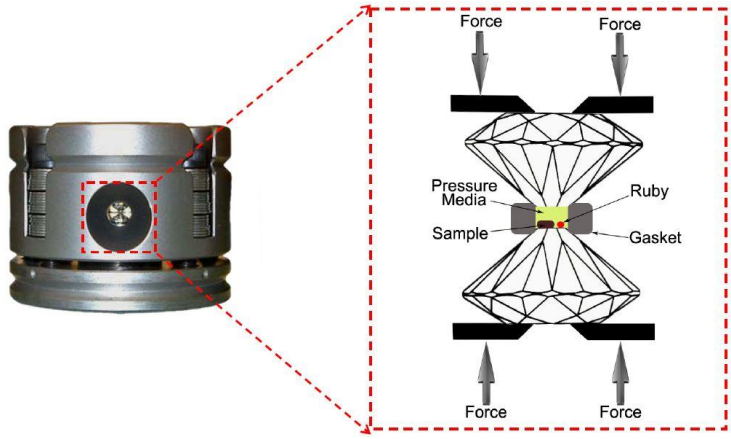

Fig 1.2.2
Schematic working principle of a diamond anvil cell

The design goal of P61.2 is to provide a new tool, a large volume press (LVP) instrument, for research of materials under extreme conditions at PETRA III. The

advantage of a LVP is its large sample size. In the case of a DAC, the typical sample size is ~0.1 mm diameter with a thickness of ~0.01mm. The possible sample size of a LVP is much larger: 1-10 mm diameter with a thickness of 0.5-10 mm. This large sample size is essentially important to study polycrystalline materials (e.g., grain boundary diffusion) or properties showing grain size dependence (e.g., deformation mechanism). A very important paper was published in 2013 to report earthquake analogs recorded in the laboratory using a LVP [1] (Fig 1.3.1). This study opened a new research area, “experimental seismology”, to study mechanisms of deep-focus earthquakes. Combination of knowledge obtained from such experiments and seismological observations helps to better understand earthquake mechanisms. In addition, LVPs have been used to synthesize industrial materials. Recently, nano-polycrystalline diamond has been successfully produced in industry [2, 3] with LVP techniques at pressures up to 15 GPa (Fig. 1.3.2). Researchers have reported many new nano-polycrystalline materials synthesized in LVP instruments [4-6] (Fig. 1.3.3). The industrial use of LVPs may become more popular in the near future.

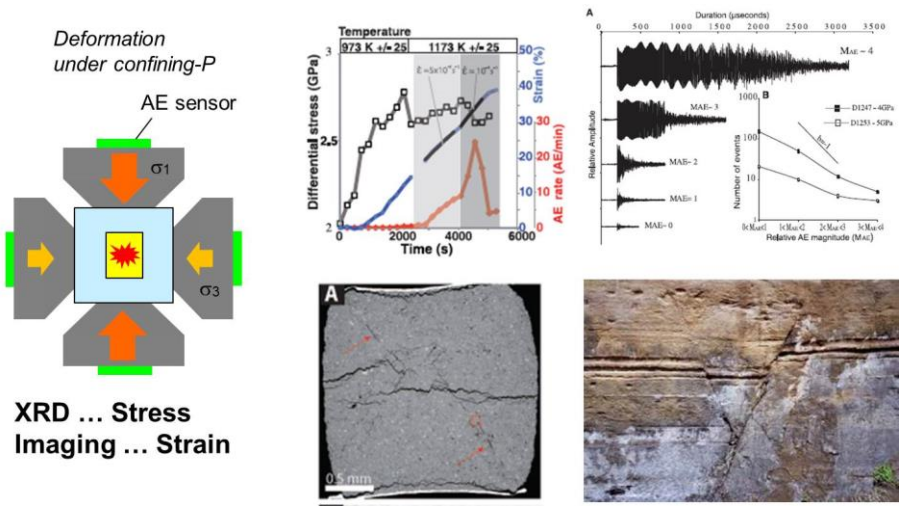

Fig. 1.3.1
Earthquake analogs recorded in the laboratory using a LVP (*Schubnel et al., Science, 2013*)

Fig 1.3.2
Nanopolycrystalline diamond

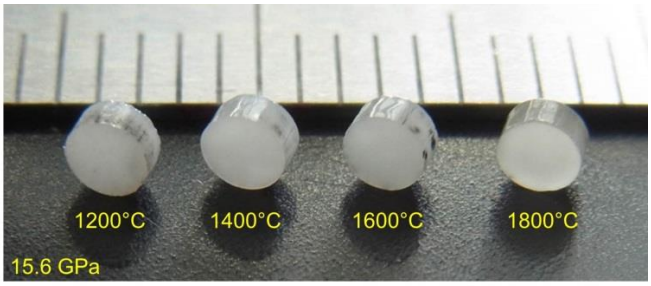

Fig 1.3.3
Nano-polycrystalline stishovite (SiO_2) synthesized with a LVP

References

[1] Schubnel A, Brunet F, Hilairet N, Gasc J, Wang Y, and Green II HW (2013) Deep-focus earthquake analogs recorded at high pressure and temperature in the laboratory. *Science* **241**, 1377-1380.

[2] Irifune T, Kurio A, Sakamoto S, Inoue T, and Sumiya H (2003) Ultrahard polycrystalline diamond from graphite. *Nature* **421**, 599-600.

[3] Sumiya H and Irifune T (2004) Indentation hardness of nano-polycrystalline diamond prepared from graphite by direct conversion. *Diamond & Related Materials* **13**, 1771-1776.

[4] Huang Q, Yu D, Xu B, Hu W, Ma Y, Wang Y, Zhao Z, Wen B, He J, Liu Z, and Tian Y (2014) Nanotwinned diamond with unprecedented hardness and stability. *Nature* **510**, 250-253.

[5] Tian Y, Xu B, Yu D, Ma Y, Wang Y, Jiang Y, Hu W, Tang C, Gao Y, Luo K, Zhao Z, Wang LM, Wen B, He J, and Liu Z (2013) Ultrahard nanotwinned cubic boron nitride. *Nature* **493**, 385-388.

[6] Nishiyama N, Seike S, Hamaguchi T, Irifune T, Matsushita M, Takahashi M, Ohfuji H, and Kono Y (2012) Synthesis of nanocrystalline bulk SiO2 stishovite with very high toughness. *Scripta Materialia* **67**, 955-958.

2. Beamline and X-ray optics

2.1 Layout and overview

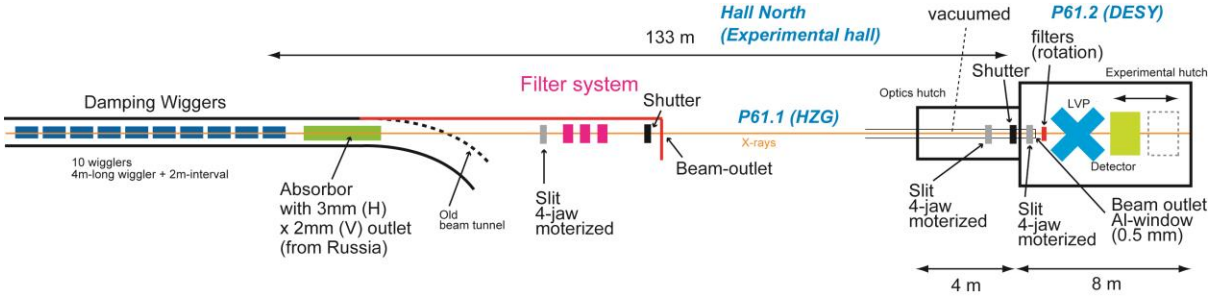

Fig. 2.1.1

A schematic beamline layout, hutches of P61.1 are not shown for clarity

The overall layout of beamline P61.2 is schematically shown in Fig. 2.1.1. The X-ray source is an array of ten 4m long fixed-gap damping wigglers which serve to reduce the machine emittance. The powerful white beam from these insertion devices will be filtered by an absorber unit to reduce the total power load on the downstream optical elements. Essentially, the low-energy part of the spectrum (below about 40 keV) will be cut off. It is noted that more than 50% of the total emitted power will still present in the high-energy spectrum. The beam size will be adjusted by a high-power slit system in an optics hutch. The filtered white beam (“pink” beam) will then be guided to the experimental hutch downstream.

Fig. 2.1.2 shows the schematic beamline floor plan in the new experimental hall north (PXN). Beamline P61 is located in sector 1, beamlines P62/P63 in sector 2 will not be built in the current phase of the PETRA III extension project and sector 3 accommodates undulator beamlines P64/P65 for x-ray absorption (XAFS) experiments. Laboratory space including preparation facilities are available in the experimental hall on the ground floor, offices for beamline staff and guests are available on the second floor. Beamline P61 is designed to serve two communities. Upstream, experimental hutch P61.1 will accommodate instrumentation for high-energy engineering materials science experiments relocated from the former DORIS III facility. These instruments will be operated by Helmholtz-Center Geesthacht (HZG). Hutch P61.2 for the LVP instrument is located downstream. Both communities share the same beamline frontend and the beamtime is split. The downstream location of the LVP instrument allows off-line operation when x-ray beam is provided to the P61.1.

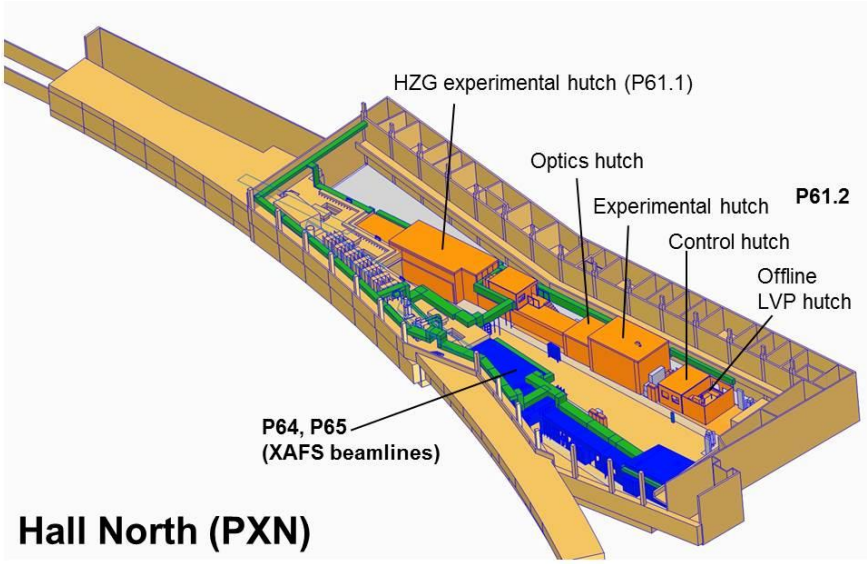

Fig. 2.1.2
Floor plan of experimental hall north (PXN) showing the arrangement of hutches along beamline P61 in sector 1. The blue area indicates the experimental facilities in sector 3.

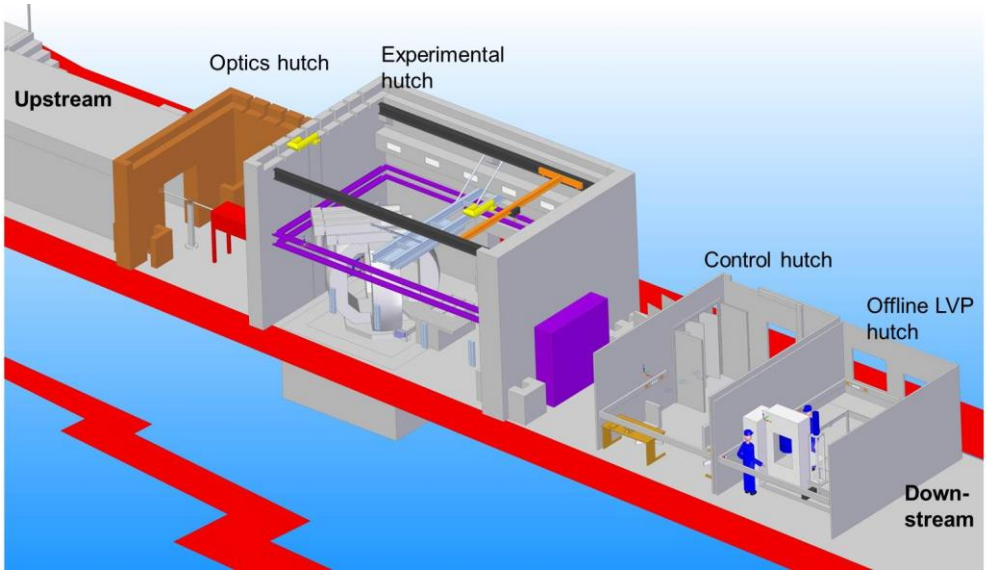

Fig. 2.1.3
Close-up view of the experimental hutches of P61.2. The position of the offline instrument is also indicated.

Fig. 2.1.3 shows the different hutches for P61.2. We will have an optics hutch, an experimental hutch, and a control hutch. The experimental hutch has a pit with 3m x 3m lateral dimension and 1.2m depth with a separate foundation to accommodate the heavy LVP instrument. A steel frame structure was embedded into the bottom of the

pit (Fig. 2.1.4) onto which the LVP will be mounted. Inside the hutch, a hoist crane (1000 kg) will be available e.g. for maintenance of the hydraulic systems that are situated on the top of the LVP instrument. An additional hutch at the end of the beamline will house the ex-situ LVP (mavo press LPR 1000-400/50, Max Voggenreiter GmbH) which is already present. It was acquired using funds from a research budget supported by Japan Science and Technology agency (JST). This instrument has been under operation since May 2013 (Fig. 2.1.5) in the former main DORIS hall and will finally be relocated to P61.2 in extension hall north. When there is no X-ray beam at P61.2 during operation of P61.1, both LVP instruments will be used off-line to synthesize materials under high pressure and high temperature which may also be analyzed using other PETRA III beamlines.

Fig 2.1.4
View into the pit for the in-situ LVP at P61.2 showing the embedded steel frame structure later supporting the heavy instrument

Fig. 2.1.5
Additional LVP instrument (mavo press LPR 1000-400/50, Max Voggenreiter GmbH) for ex-situ experiments and materials synthesis currently operated in the former DORIS hall

2.2 Damping wigglers

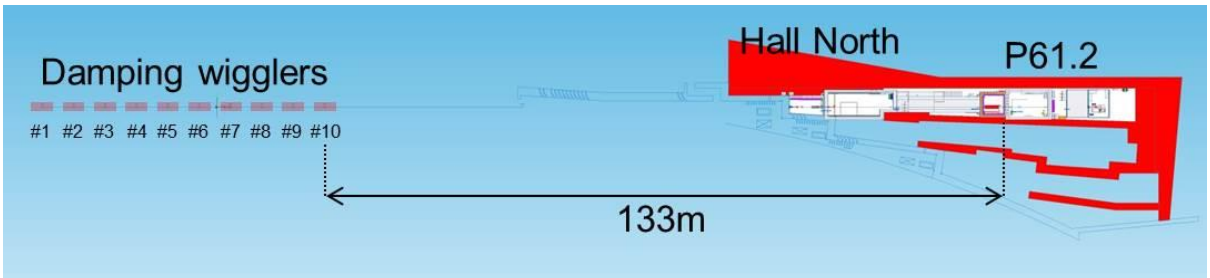

Fig. 2.2.1
Schematic of the damping wiggler array relative to the LVP location at P61.2

The X-ray source of P61.2 is an array of damping wigglers located in the northern long straight section of the 6 GeV PETRA III storage ring whose primary purpose is to reduce the machine emittance to 1 nmrad. For P61 these damping wigglers will serve

as a powerful source of a high-energy white X-ray spectrum (Table 2.2.1). The damping wigglers consist of ten independent fixed-gap wigglers, 4m long each and separated by 2m (Figs. 2.2.1 and 2.2.2). The distance from the center of the last 10th wiggler to the end of the optics hutch is 133 m. Fig. 2.2.3 shows the calculated flux as a function of the X-ray energy at the end of the optics hutch (133 m from the center of

Peak field B_0	1.52 T
Magnetic gap	24 mm
Period length λ_U	200 mm
Number of poles	40 = 36 + 2 (0.75B_0) + 2 (0.25 B_0)

Table 2.2.1
Damping wiggler parameters

the last wiggler) through a 1mm x 1mm slit. For comparison, the corresponding flux of bending magnet beamline BL04B1 at SPring-8 is shown where also a LVP instrument is operated. The source to sample distance at the Spring-8 beamline is considerably smaller than at P61.2. The power wigglers at P61.2 however still provide a flux about ten times higher than at BL04B1. Fig. 2.2.4 shows the flux ratio of both beamlines as a function of X-ray energy showing that the P61 beam is increasingly powerful at higher energies.

Fig. 2.2.2
View of the damping wiggler array in the northern long straight section of PETRA III

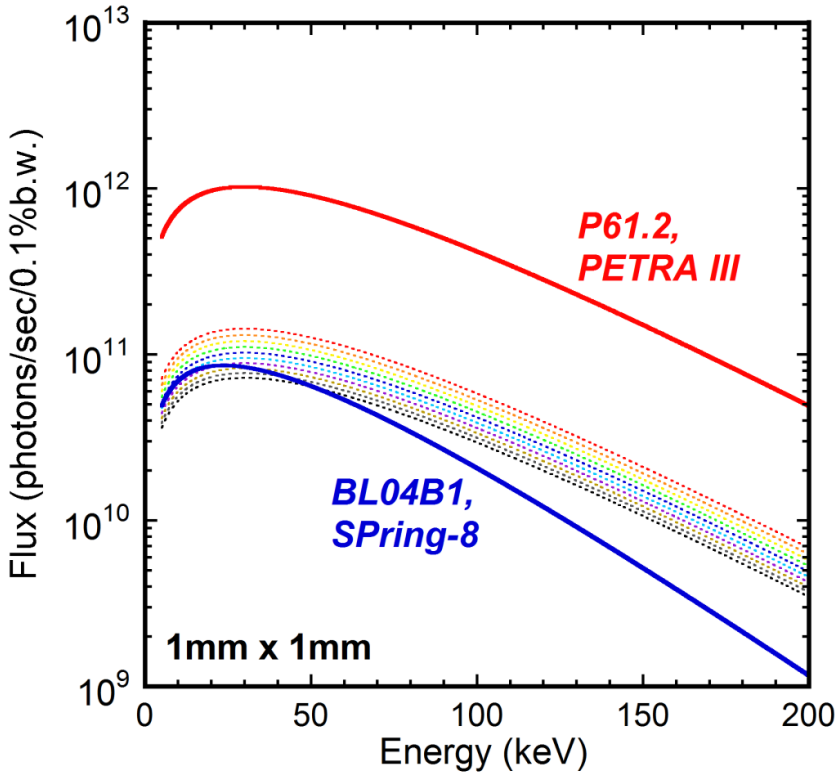

Fig. 2.2.3

Total flux of the damping wigglers at P61.2 through a 1mm x 1mm slit at the LVP position (red line). For comparison, the flux at BL04B1 (SPring-8) is shown for the same aperture at the LVP location (blue line). A dotted line represents flux from each wiggler that consists of damping wiggler section.

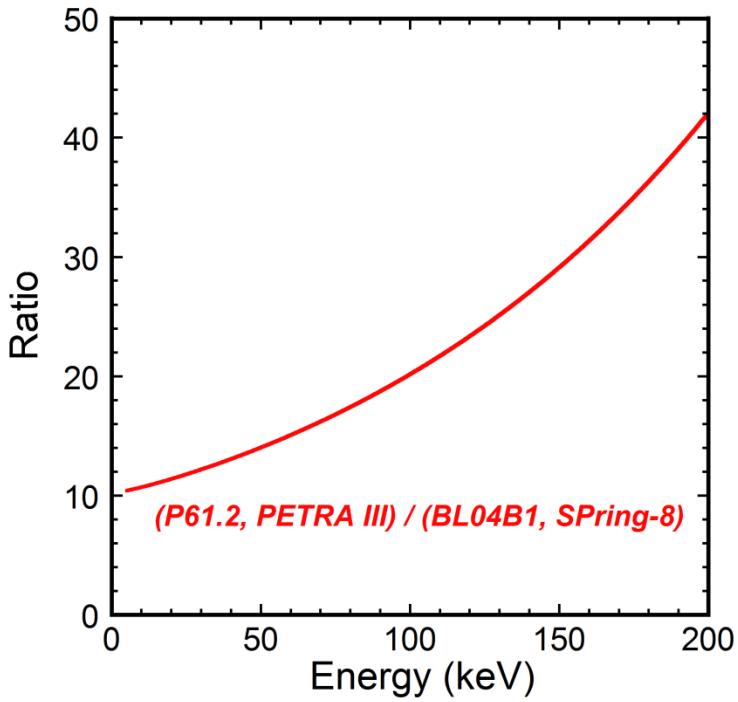

Fig 2.2.4

Flux ratio of the spectra plotted in Fig. 2.2.3

2.3 Frontend

2.3.1 Overview

Figure 2.3.1 shows a drawing of the whole view of front end components. The girder concept is generally employed in PETRA III and PETRAIII extension project. In P61.2, the front end components consist of three girders. The purpose of the frontend components is management of heat load of white beam from damping wigglers.

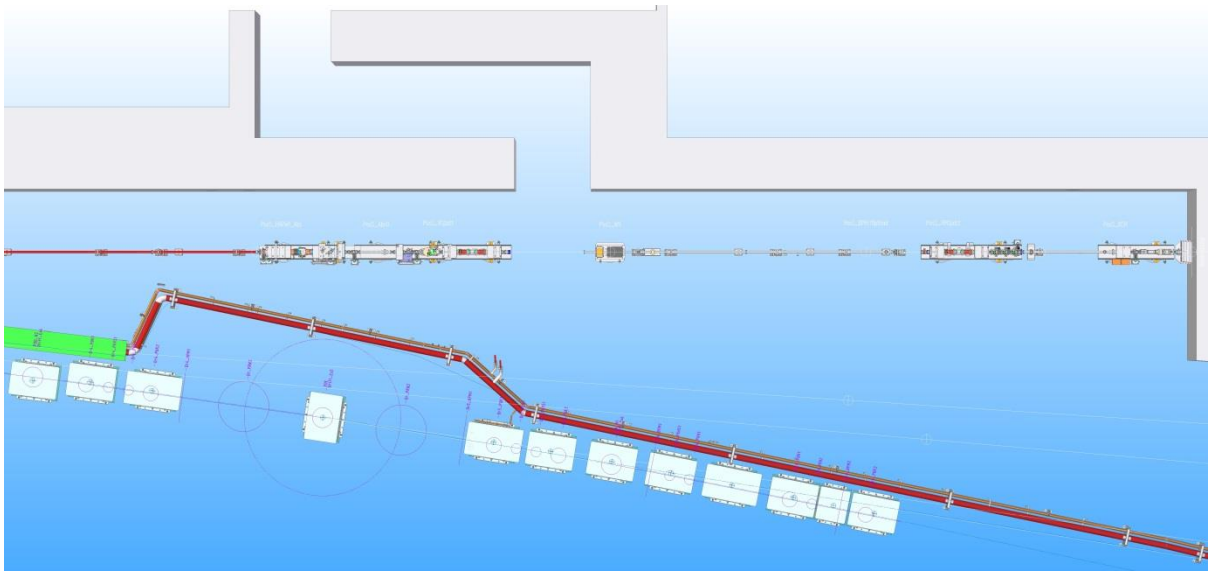

Fig. 2.3.1
Schematic view of the frontend of P61.2 (components along the straight beamline at the top). PETRA III storage ring magnets are seen below.

2.3.2 Damping wiggler beam absorber

The full damping wiggler beam is currently completely absorbed by a long water-cooled inclined surface copper absorber unit. The end segment of this absorber will be replaced by a modified one having a rectangular on axis hole (3mm horizontal x 2mm vertical) as a beam outlet. This component is currently being constructed by Budger Institute (Nowosibirsk, Russia) and will be installed end of 2016. Fig. 2.3.2 shows a photo of the current absorber for the dumping wiggler without the beam outlet.

Fig 2.3.2
The current copper absorber unit for the dumping wigglers, end piece removed.

2.3.3 Filters

Figure 2.3.3 shows the frontend girder with pre-assembled and aligned high-power slits and three filter units. One unit has two positions for different filters. We are planning to use a filter made of 300 μm CVD diamond with 50 μm Cu. The minimum is one filter (300 μm diamond + 50 μm Cu); the maximum is three filters (900 μm diamond + 150 μm Cu).

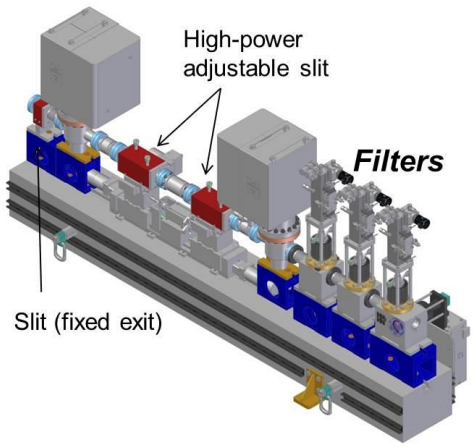

Fig 2.3.3
Frontend girder with high-power slits and filter units.

Fig. 2.3.4 shows the resulting filtered photon flux which is strongly reduced below 40 keV bringing the total power in the beam down to a tolerable level. The minimum filter (300μm CVD-diamond + 50μm Cu) will be used for energy dispersive X-ray diffraction measurements; the minimum filter (900μm CVD-diamond + 150μm Cu) will be used for studies using monochromatic X-rays.

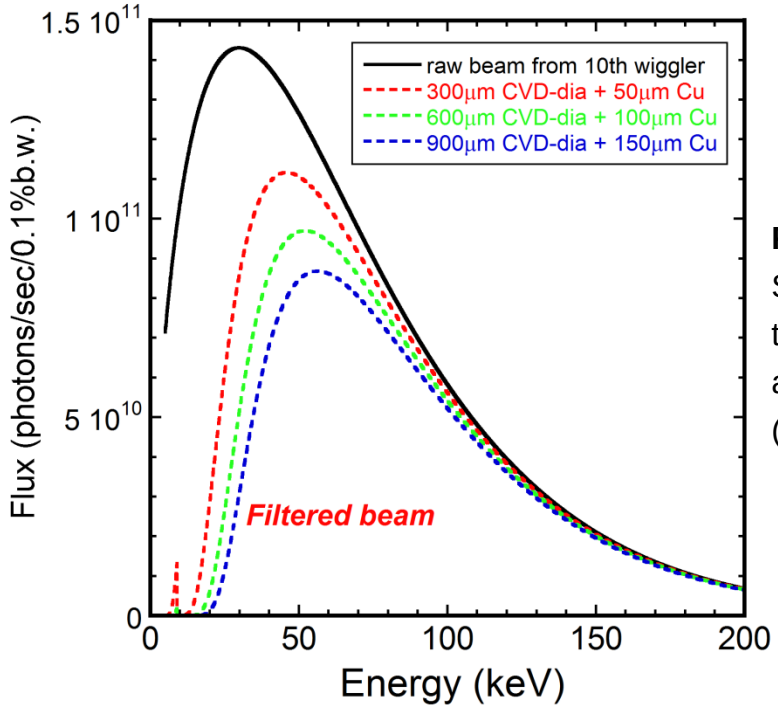

Fig 2.3.4
Spectral distribution of the filtered beam. Data are shown only for last (10^{th}) wiggler.

2.3.4 Shutter and beam-outlet

Figure 2.3.5 shows frontend girder 3 that holds a beam shutter unit. Behind the shutter there is a lead collimator (200 mm thick) to cut unnecessary scattering produced in the front end.

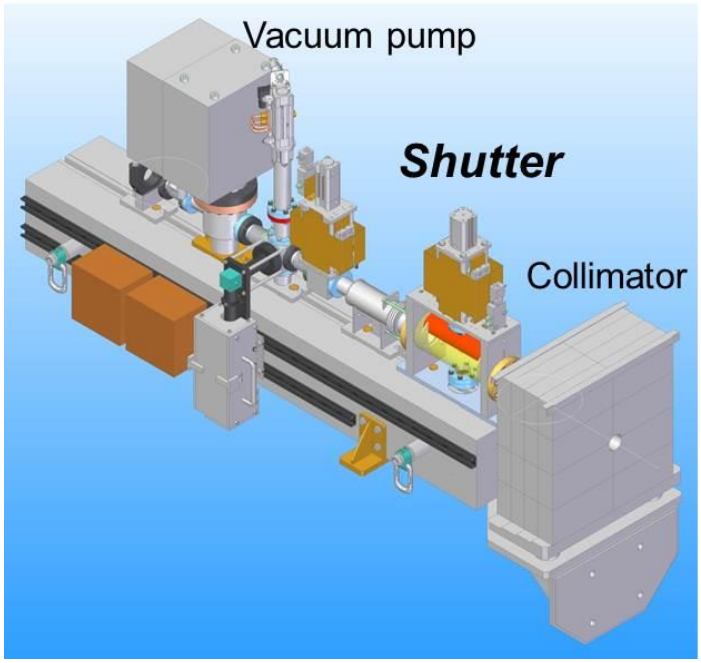

Fig 2.3.4
Girder 3 with a shutter unit.

2.4 Optics hutch

2.4.1 Overview

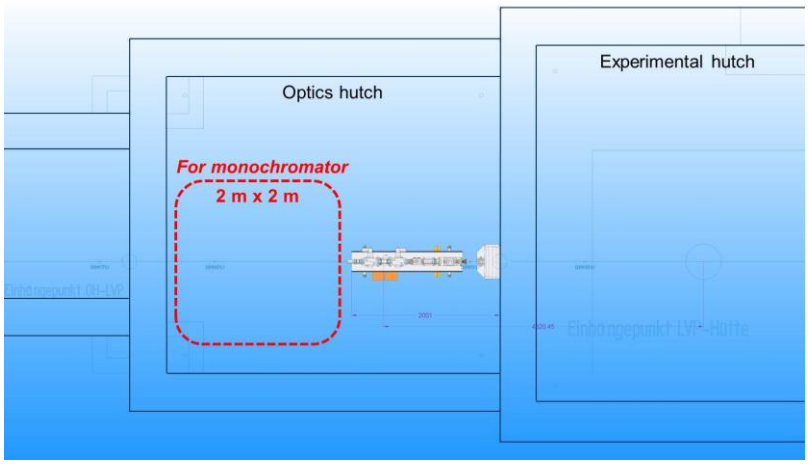

Fig 2.4.1
Layout of components in the optics hutch

An optics hutch of P61.2 is located in front of the experimental hutch. Fig. 2.4.1 shows a layout of components in the optics hutch. Here, a high-power xy slit system will be used to adjust the size of the filtered white beam from the damping wigglers. There is also space available to install a Laue monochromator as a future upgrade of the beamline. Fig. 2.4.2 shows a schematic illustration of a girder that will be located in the optics hutch. This has a high-power adjustable xy slit system and a shutter component. At the very end of the optics hutch, a lead collimator is located.

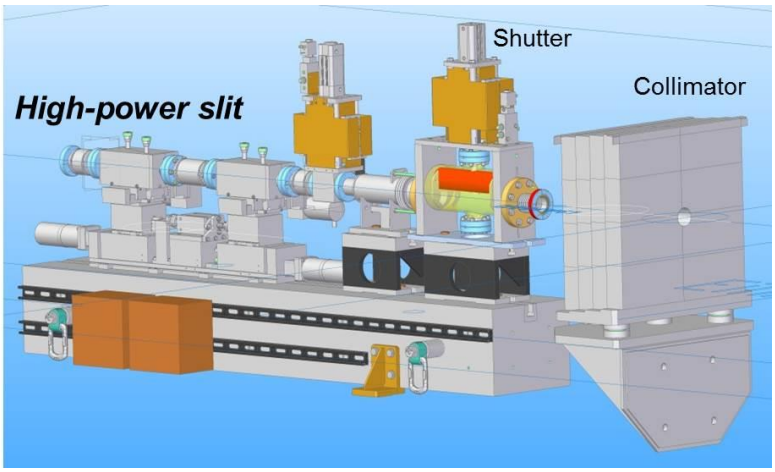

Fig 2.4.2
Frontend girder with high-power slits and beam shutter which will also be installed in the optics hutch

2.4.2 High-power xy slit system

Figure 2.4.3 shows a high-power adjustable xy slit system. There are two boxes for this system. A box has a metal piece with a rectangular hole with 10 mm in horizontal and 6 mm in vertical (Fig. 2.4.4). The metal piece is attached to a copper piece that is cooled by water flow. Fig. 2.4.5 shows a view of the slit system along the X-ray direction. The two rectangular holes do not overlap when the two boxes are located at

the original positions, i.e. the beam is completely blocked. Translating the units relative to each other allows to define an effective opening by the overlapped area of the rectangular holes. The maximum opening is 10 mm horizontal and 6 mm vertical.

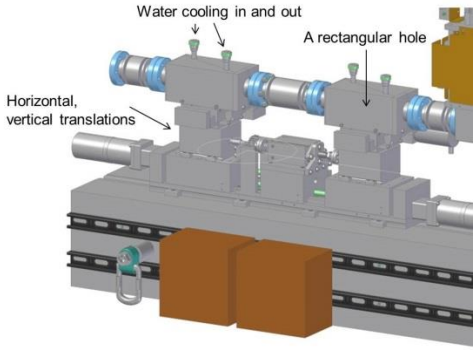

Fig 2.4.3
High-power adjustable xy slit

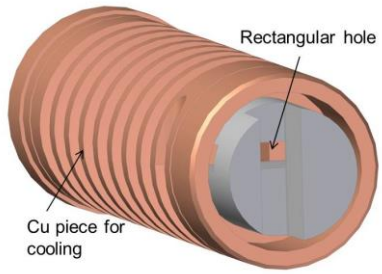

Fig 2.4.4
Rectangular slit, opening 10mm (H), 6mm (V)

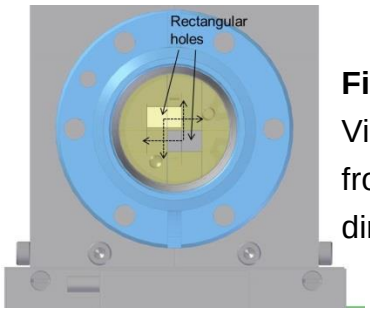

Fig 2.4.5
View of xy-slit from the X-ray direction

2.4.3 Shutter and collimator

A shutter unit is located on this girder (Fig. 2.4.2). The shutter unit is linked with the high-power xy-slit. When the shutter is closed, the xy-slit boxes are also moved to the original positions to close the opening of the slit. The thickness of the collimator is 200 mm. This is four times thicker than those of other PETRA III beamlines.

2.5 Experimental hutch

2.5.1 xy-slit system and beam-outlet

A high-power xy-slit system that is the same as that is installed in the optics hutch (Fig. 2.4.3) is installed in the experimental hutch. The vacuum pipe is introduced into the experimental hutch. The beam outlet from the vacuum pipe is an aluminum window with 0.5 mm thickness, the corresponding X-ray transmission is shown in Fig. 2.5.1.

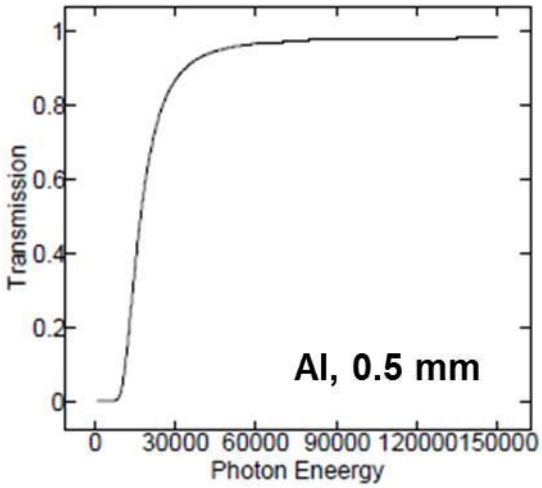

Fig 2.5.1
Transmission of the terminating Al window (thickness 0.5mm)

2.5.2 Additional filters

An additional filter system will be installed in the experimental hutch. This component will be installed between the beam outlet and the LVP. These additional filters will be mainly used to reduce the beam intensity when a broader beam is used for imaging experiments.

3. LVP instrument for P61.2

3.1 Overview

The LVP instrument that will be installed at the beamline has six hydraulic rams to control six anvils independently. This type of instrument is called a 6-rams-LVP. The first modern 6-rams LVP was built in the Institute for Study of the Earth's Interior, Okayama University [1] (Fig. 3.1.1). Today, four instruments are under operation worldwide: two in Germany and two in Japan. Up to now, this type of instrument had been installed at neutron facilities in Germany (MLZ) and Japan (JPARC) for neutron diffraction measurements under high-pressure and high-temperature conditions. The instrument that will be installed in P61.2 will be the world's first 6-rams-LVP operated at a synchrotron facility.

This type of instrument has several advantages as a LVP instrument:

- Deformation capability
- Precise control of anvil positions
- High efficiency of pressure generation
- Large access angle to a sample under high pressure and temperature

For deformation experiments under high pressure and temperature, the most popular instrument is deformation-DIA (DDIA) [2]. Many DDIA presses have been under operation in major synchrotron facilities. We can also deform the sample under high pressure and temperature using the 6-rams-LVP because all the six anvils are controlled independently.

For modern 6-rams-LVP, the positions of the anvils can be measured allowing their precise control during compression and decompression. This has the advantage to keep cubic geometry of the pressurized space. This allows using sintered diamond anvils as the second stage anvils [1] which will expand the pressure range of the experiments. The highest pressure generated using a LVP with sintered diamond anvils so far is 109 GPa [3].

Fig. 3.1.2 shows load vs. pressure curves determined by a DIA-type apparatus and by a 6-rams-LVP. This result shows that pressure generation of the 6-rams-LVP is 10% more efficient than that of the DIA-type apparatus. In the DIA-type apparatus, friction between guide blocks and sliding blocks makes the load vs. pressure curve less efficient.

Since the 6-rams-LVP does not have guide blocks, the access angle to the sample located at the center of the instrument is larger than those of other types of high-pressure apparatus which is beneficial for X-ray diffraction measurements under high-pressure.

Fig 3.1.1
A 6-rams-LVP at the Institute for Study of the Earth's Interior, Okayama University.

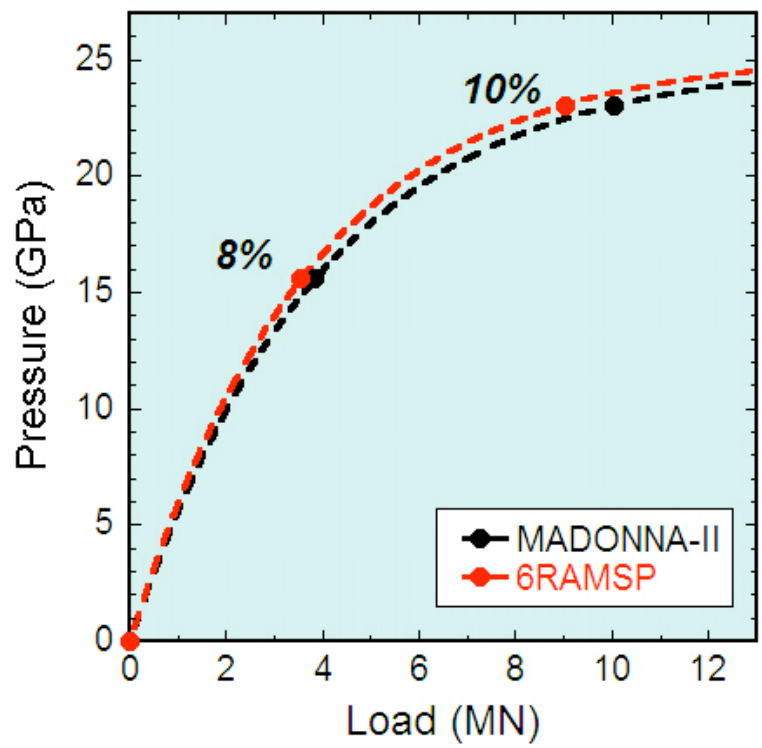

Fig 3.1.2
Load vs. pressure curves of a 6-rams-LVP (6RAMSP) and a DIA-type apparatus (MADONNA-II)

3.2 6-rams LVP instrument

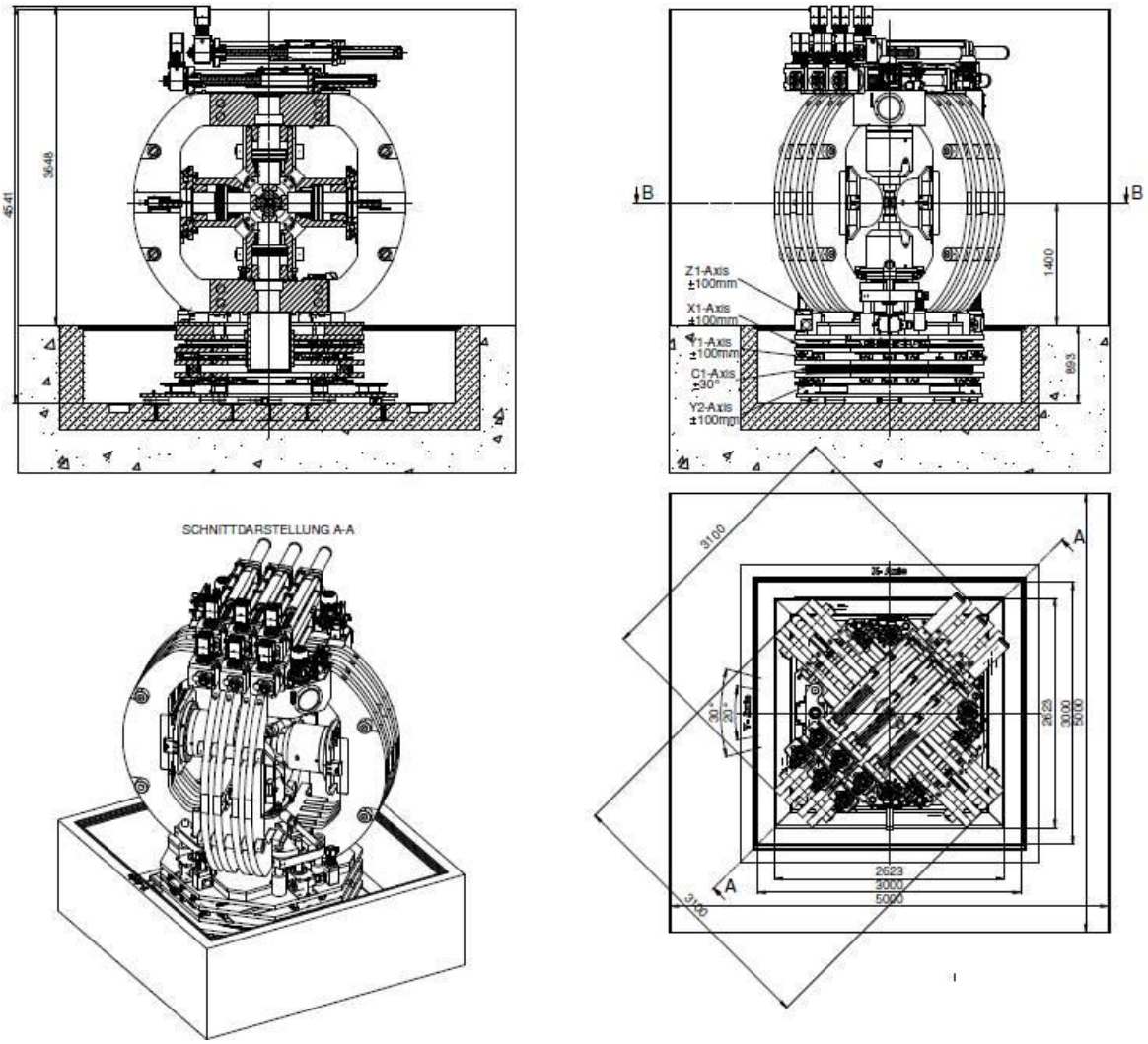

Fig. 3.2.1 Drawings of the 6-rams-LVP for P61.2

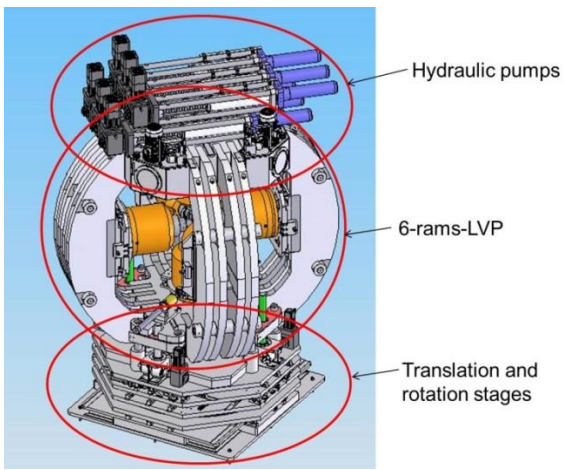

Fig 3.2.2
A schematic illustration of the 6-rams-LVP

Fig. 3.2.1 shows drawings of the 6-rams-LVP that will be installed at P61.2, a schematic illustration is shown in Fig. 3.2.2. This instrument consists of three main parts: hydraulic pumps on the top; 6-rams-LVP in the middle; translation and rotation stages at the bottom.

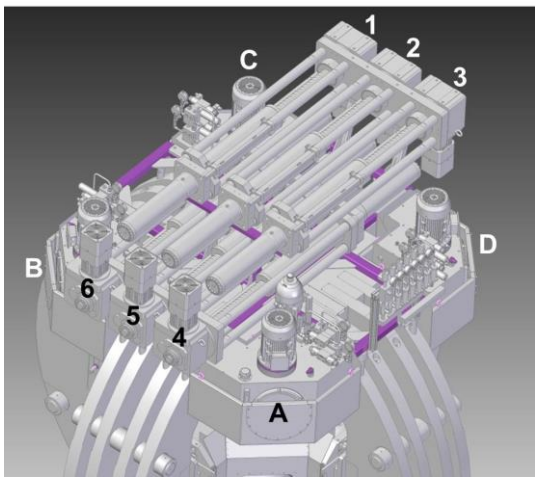

Fig 3.2.3
Hydraulic pumps on the LVP instrument.
1-6: pressure intensifiers
A-D: low-pressure pumps

Figure 3.2.3 shows the hydraulic pumps that are located on the 6-rams-LVP instrument. Six long pumps (1-6 in Fig. 3.2.3) are the pressure intensifiers for the high oil-pressure region. Each pump is connected to each hydraulic ram in order to control oil pressures independently. There are four low-pressure pumps which are used to adjust the piston positions at low oil-pressure. The positions of the instruments will be moved during the measurements in order to adjust the sample position to the beam and the sample can be oscillated during the measurements. Since these hydraulic pumps are located on the instrument, steel pipes (rigid) are used for connection between hydraulic rams and pumps. Then, the effect of expansion of the oil pipes during operation of the 6-rams-LVP instrument can be minimized. The maximum oil-pressure is 630 bar.

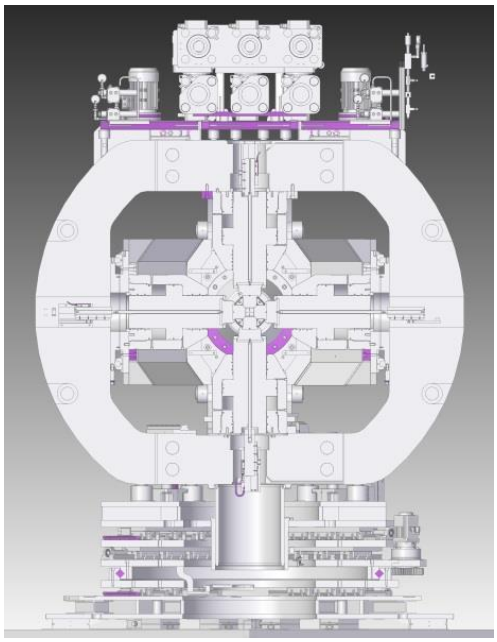

Fig 3.2.4
Cross section of the 6-rams-LVP.

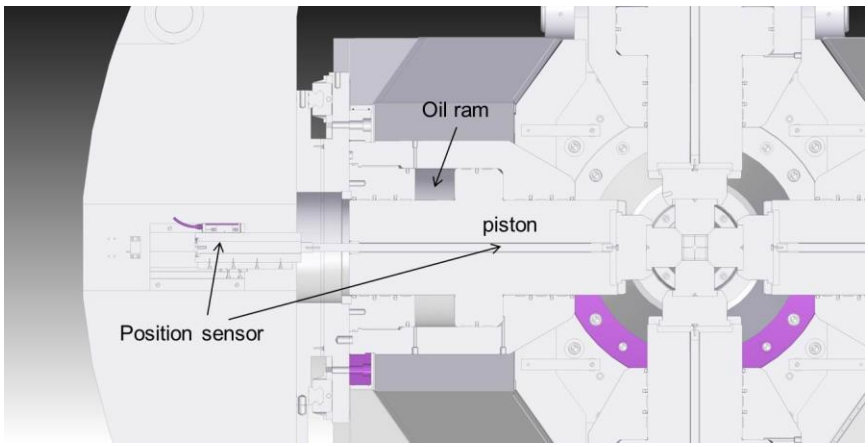

Fig 3.2.5
Enlarged view of a position sensor

Fig. 3.2.4 shows an illustration of a cross section of the 6-rams-LVP. Fig. 3.2.5 shows an enlarged view of a position sensor for the first stage anvil. There is a hole inside of the piston. A rod is located in this hole and an end of the rod is fixed to the bottom of the first stage anvil. The other end is fixed to a sensor unit to measure the position. The reading device for the sensor unit is fixed to the press frame. There are six sensor units for all of the pistons and the first stage anvils. Then, we can measure positions of the first stage anvils relative to the press frame during compression and decompression of the instrument. Elastic deformation of the press frame will also be measured as a function of oil pressure. Using these data, we can compensate the elastic deformation of the press frame which affects the positions of the reading devices for the sensors. Then, we can determine absolute positions of the first anvils

during the operation.

The maximum force generated is 500 tons for each piston. This 6-rams-LVP is almost equivalent to a 1500-ton DIA type press, which are in operation at SPring-8 and ESRF. The edge length of the first stage anvil is 60 mm. It is planned to use WC anvils with edge length of 27 mm for higher pressure experiments using sintered diamond anvils (14 mm cubes).

The 6-rams-LVP instrument for P61.2 is funded by the Federal Ministry of Education and Research (BMBF) within a project of University of Bayreuth (KEI0500009612, 07.2013-06.2016) lead by Prof. Tomoo Katsura.

3.3 LVP stage

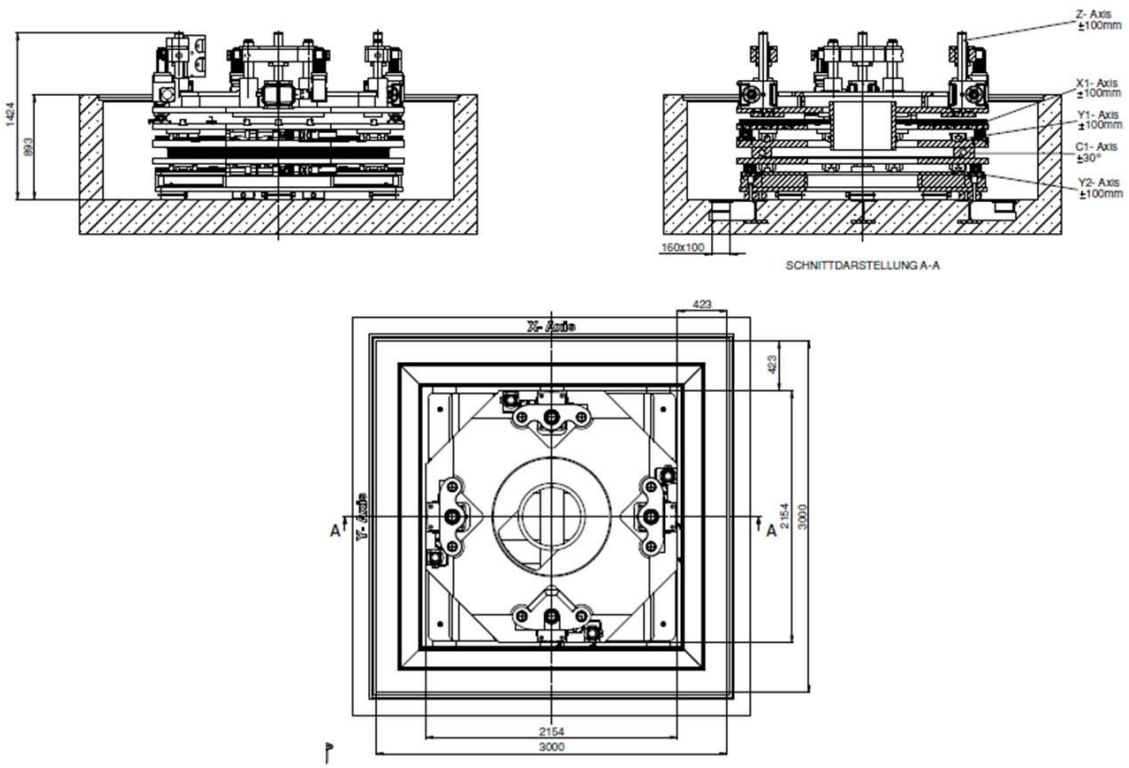

Fig. 3.3.1 Stages for the 6-rams-LVP

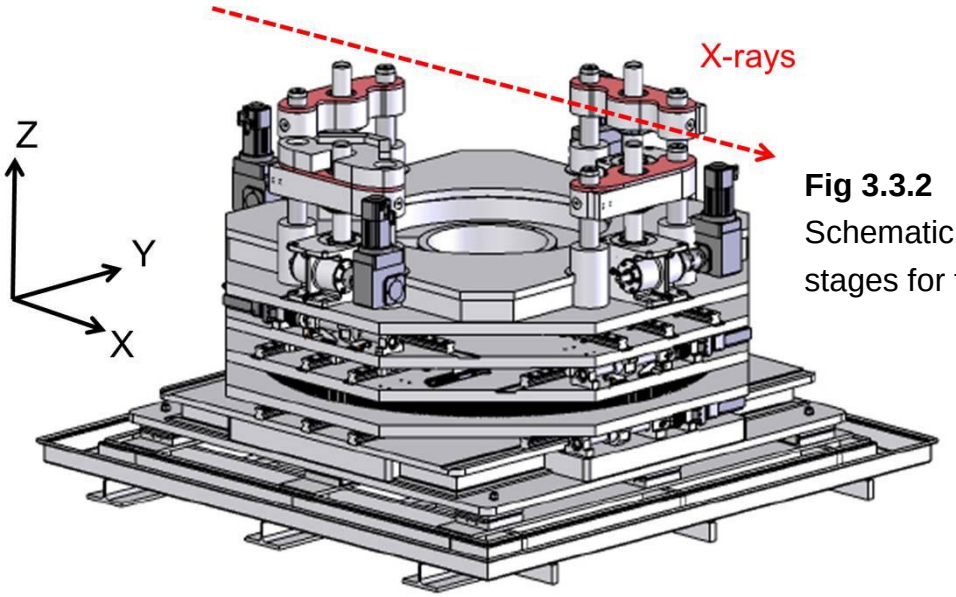

Fig 3.3.2
Schematic illustration of the stages for the 6-rams-LVP

Fig. 3.3.1 shows drawings of a stage system for the 6-rams-LVP. A schematic illustration (Fig. 3.3.2) also shows the xyz directions for the stages. The X-rays pass through the instrument along the X direction. Y is the horizontal and Z is the vertical direction. This stage system has one rotation and four translations. The specifications are (from bottom to top):

- Y2 axis: ± 100 mm. The purpose of this axis is to align ϕZ to the beam.
- ϕZ: ± 30 degrees. This rotation stage enables to oscillate the sample under high PT conditions to increase the number of grains that contribute diffracted X-rays. The rotation axis is also useful to align anvil gaps relative to the beam.
- Y1: ± 100 mm to adjust the sample position along the Y direction.
- X axis: ± 100 mm to adjust sample position along the X direction.
- Z axis: ± 100 mm to adjust sample position along the Z direction.

All translations and the rotation stage are driven by servo motors connected to vendor specific drive electronics. In order to integrate the system into the PETRA III experiment control framework, specific TANGO servers for the motor control will be provided by FS-EC, the photon science experiment control group. Scanning procedures will be implemented to maximize diffracted signals automatically.

3.4 Power supply for heating

A DC power supply is used for heating under high pressure. Several kinds of heating materials will be used: metals (Pt, Ta, Re, …); $BN+TiB_2$; Graphite; $LaCrO_3$. The resistance of these materials are in a range from a few milliohm (for metals) to ~1 ohm (for $LaCrO_3$). For the low-resistance heaters, a high current of several hundred amps (at several volts) is needed, while for the high-resistance heaters it is several tens amps and tens volts. The power supply that will be used here should cover 0-several tens volts and 0-several hundred amps.

Fig. 3.4.1 DC power supply for driving the different heaters
Voltage: 0 - 40V, current 0 - 510A; max. power: 10 kW

Fig. 3.4.1 shows a DC power supply that will be used for the heaters. The maximum voltage is 40V, maximum current is 510 A and the maximum power is 10 kW. Voltage and current are freely adjustable within the power limit of 10 kW (Fig. 3.4.2). We can change the parameters in cv mode (constant voltage), cc mode (constant current), and cp mode (constant power). The power supply unit will be remotely controlled by a TANGO server integrated in the experiment control layer. This e.g. allows performing experiments with constant heating rate, i.e. constant power increase per unit time.

We are also planning to install an AC power supply. Since the thermocouple output signal is DC in the millivolt range, an AC power supply is good for measuring the thermocouple output signal (DC) separately from input power for heating (AC). The installation of an AC power supply is planned in 2016.

Technical Data	PS 9040-510 3U
Output voltage DC	0...40V
- Ripple [1]	<150mV$_{PP}$ <10mV$_{RMS}$
-Sensing compensation	~ 1V
Output current	0...510A
- Ripple [1]	<900mA$_{PP}$ <120mA$_{RMS}$
Output power	0...10000W
Efficiency	~93%
Programming U (typ.)	1mV
Programming I (typ.)	10mA
Programming P (typ.)	0.55W
Weight [2]	25.5kg
Article number	06230263

Fig 3.4.2
Specifications of the DC power supply (PS 9040-510 3U)

3.5 Compression geometry

3.5.1 Overview

Fig. 3.5.1 shows a schematic illustration of the 6-8 compression geometry for the 6-rams-LVP, the 6-6 compression geometry is shown in Fig. 3.5.2. The 6-8 compression geometry is mainly employed in the Institute for Study of the Earth's Interior (Okayama University, Japan) [1]. The second stage anvils made of sintered diamond anvils are employed to generate high-pressure exceeding 100 GPa [3]. The 6-6 geometry is preferred for deformation experiments under high pressure and temperature at BGI (University of Bayreuth, Germany) and also for neutron scattering experiments at JPARC (Japan). Using the 6-8 geometry with tungsten carbide second stage anvils, pressures up to 30 GPa can be generated, but the maximum 2Θ angle is limited to 10 degrees. On the other hand, the 6-6 geometry enables having a wider 2Θ angle up to 30 degrees, but the maximum pressure then is limited to about 10 GPa. Both types of compression geometries will be used at P61.2 depending on the specific experimental needs.

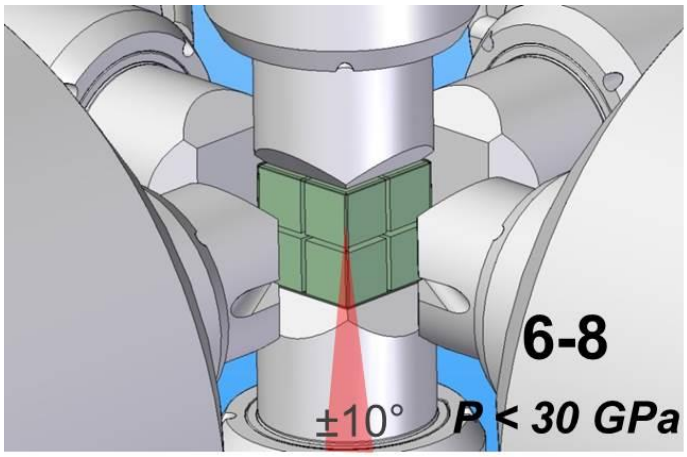

Fig 3.5.1
6-8 compression geometry for 6-rams-LVP

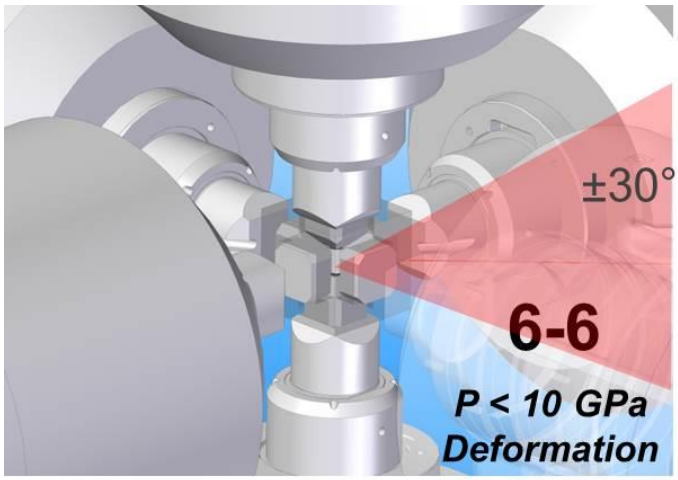

Fig 3.5.2
6-6 compression geometry for 6-rams-LVP

3.5.2 6-8 geometry

Fig. 3.5.3 shows a schematic illustration of a high pressure cell in 6-8 compression geometry. Generated pressure is controlled by the edge length of the octahedral pressure medium (OCT) and the truncated edge length (TEL) of the WC second stage anvils. Higher pressure can be generated using smaller TEL. Fig. 3.5.4 shows examples of pressure generation curves of three selected high-pressure cells (OCT/TEL = 18/11, 14/7, and 10/4). We will employ these three setups as standard high-pressure cell assemblies in P61.2 for the 6-8 geometry. Pressure ranges of these setups are

- 5-12 GPa for 18/11 cell
- 8-16 GPa for 14/7 cell
- 15-20 GPa for 10/4 cell

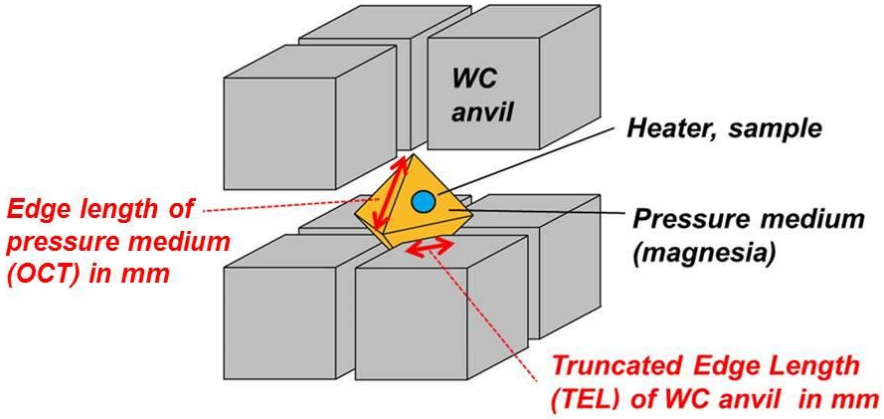

Fig. 3.5.3
A schematic illustration of a high pressure cell in 6-8 compression geometry

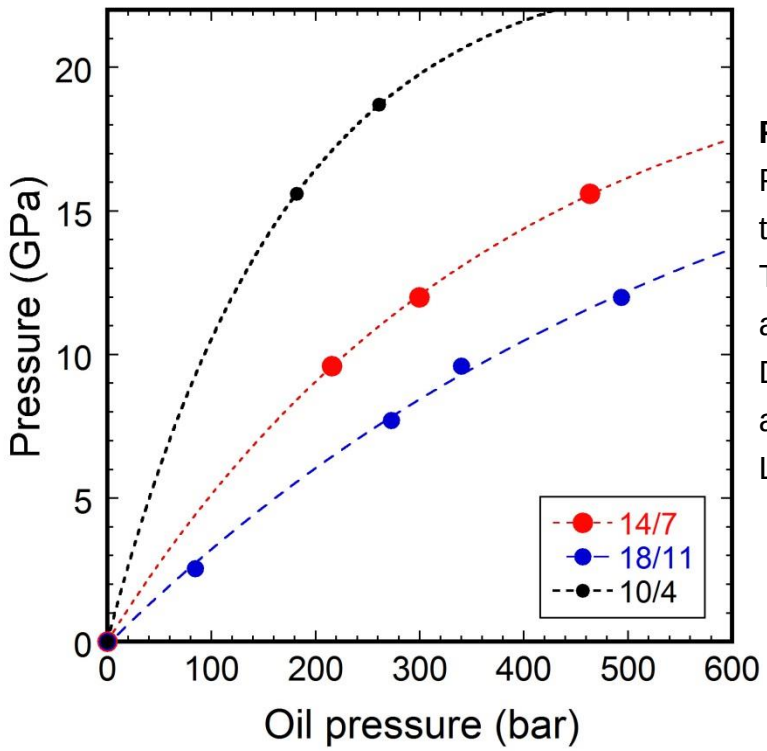

Fig 3.5.4
Pressure generation curves of three high-pressure cells. These curves were obtained for an ex-situ LVP that is installed in DORIS hall. This instrument has a Walker-module.
Load = 1.45 x oil pressure.

In the pressure range below 10 GPa, a graphite tube is employed as a heater. At pressures above 10 GPa, a BN+TiB_2 (Denka) tube is employed as a heater. Fig. 3.5.5 shows cell assemblies for 18/11 and 10/4 cells. We will carry out pressure and temperature calibration runs after installation of the 6-rams-LVP in July 2015.

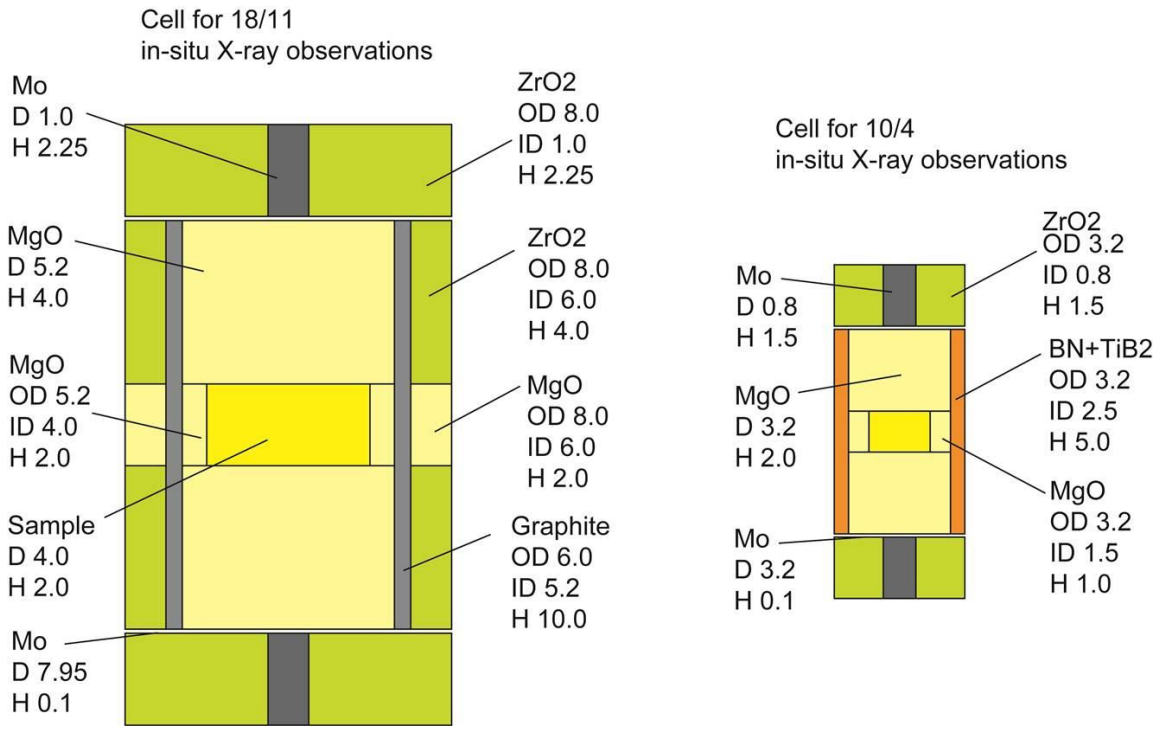

Fig. 3.5.5 High-pressure cells for in-situ X-ray observations using the 6-8 system

3.5.3 6-6 geometry

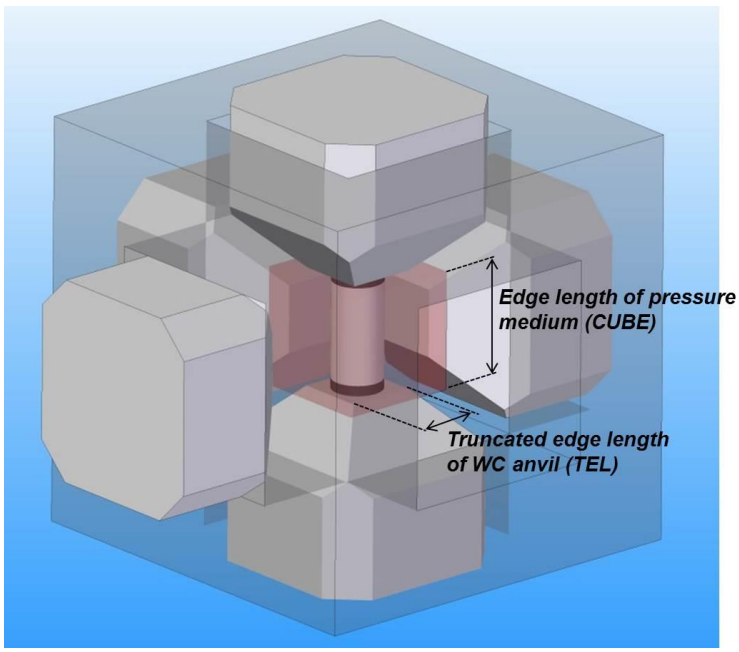

Fig 3.5.6
A schematic illustration of a high pressure cell in 6-6 compression geometry

The 6-6 compression geometry [4] has been recently employed in synchrotron facilities in Japan and neutron facilities in Germany and Japan. This compression geometry was first developed at GSECARS (Advanced Photon Source) for high-pressure experiments using synchrotron radiation [4].

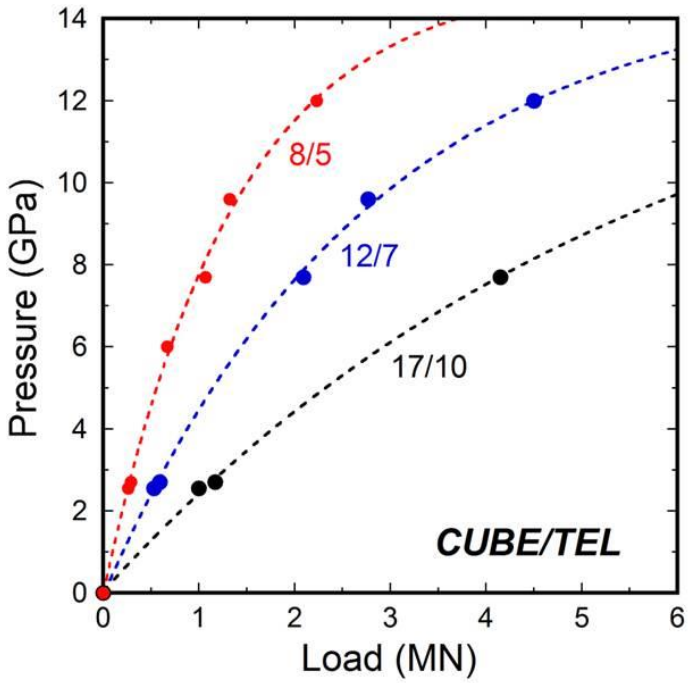

Fig 3.5.7
Pressure generation curves of 6-6 cell assemblies.

Fig. 3.5.7 shows pressure generation curves of 6-6 assemblies developed in Geodynamics Research Center (Ehime University, Japan). In JPARC, 6-6 assemblies with 17/10 and 12/7 are used as standard cell assemblies [5].

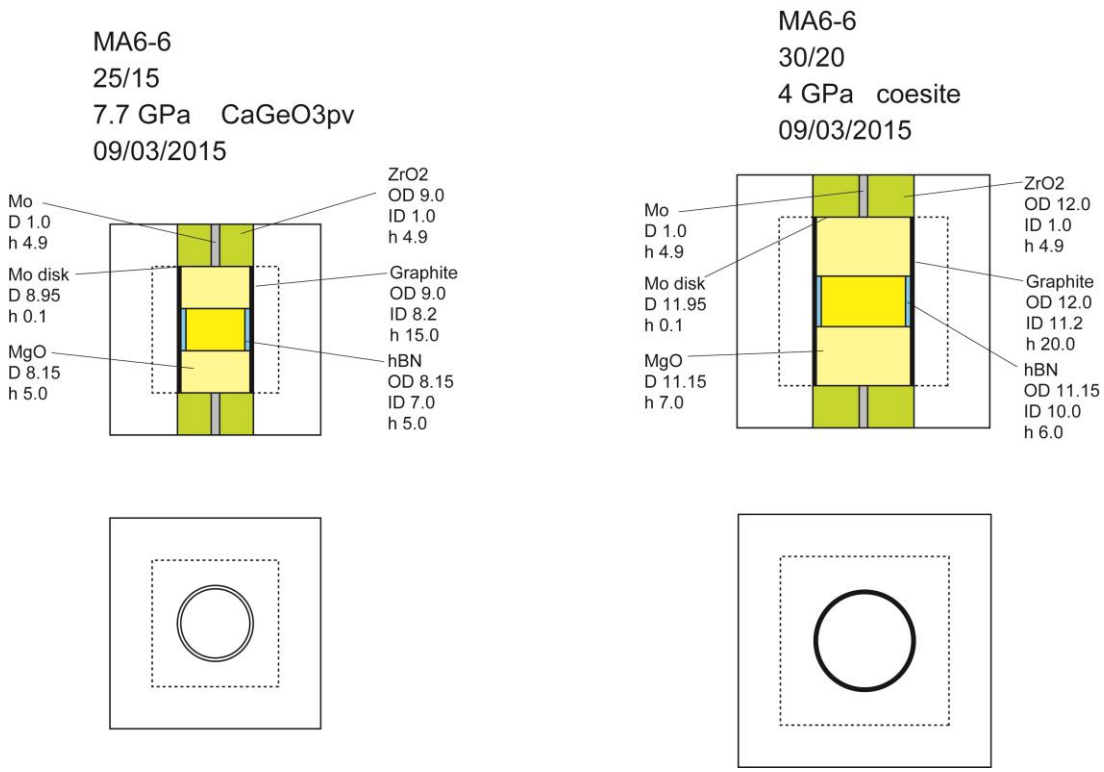

Fig. 3.5.8 High-pressure cells for in-situ X-ray observations using a 6-6 system

Fig. 3.5.5 shows cell assemblies for 25/15 and 30/20 cells. These 6-6 cell assemblies are much bigger than those in use at SPring-8 and JPARC, but are similar to those employed in the Japanese materials science community. Diameters of the sample for 25/15 and 30/20 cells are 7 and 10 mm, respectively. A Pressure up to 8 GPa can be generated using a 25/15 cell. The 30/20 cell is for experiments at lower pressures up to 4 GPa.

Fig. 3.5.9 and Fig. 3.5.10 show drawings of a 6-6 anvil and a 6-6 frame. Fig. 3.5.11 shows 3D views of the large 6-6 cell assemblies at P61.2. Fig. 3.5.12 shows a comparison of 6-6 assemblies that are employed in SPring-8, JPARC, and PETRAIII.

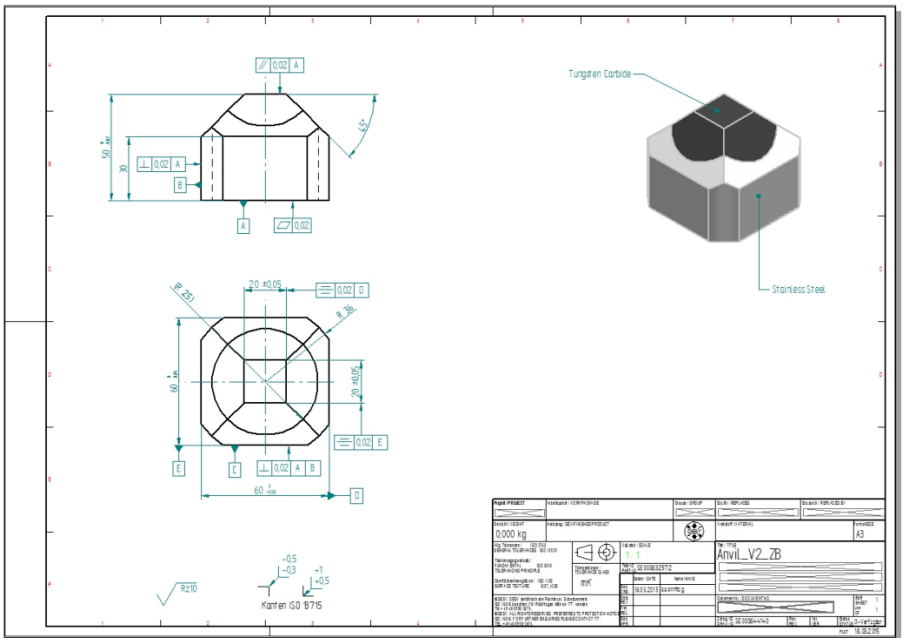

Fig. 3.5.9 6-6-anvil for P61.2

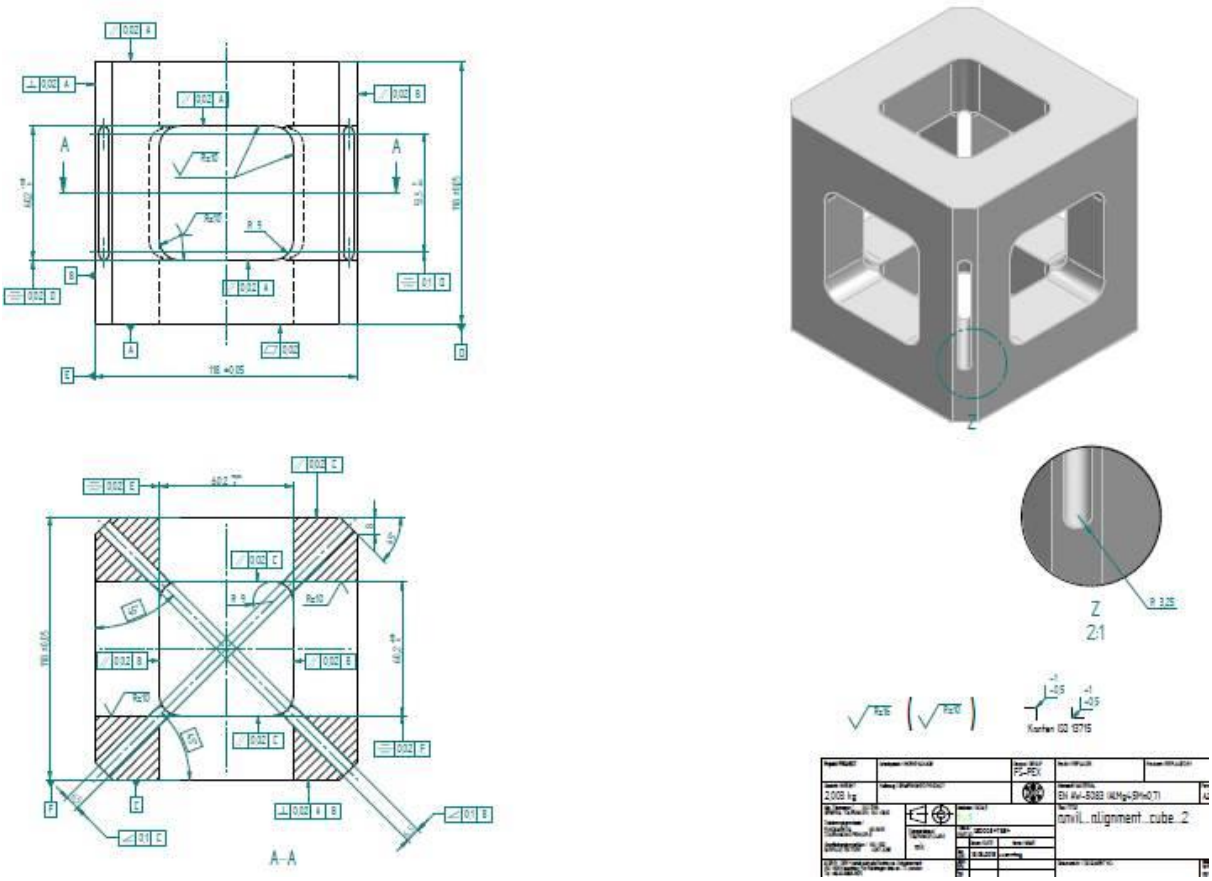

Fig. 3.5.10 Anvil alignment frame for P61.2

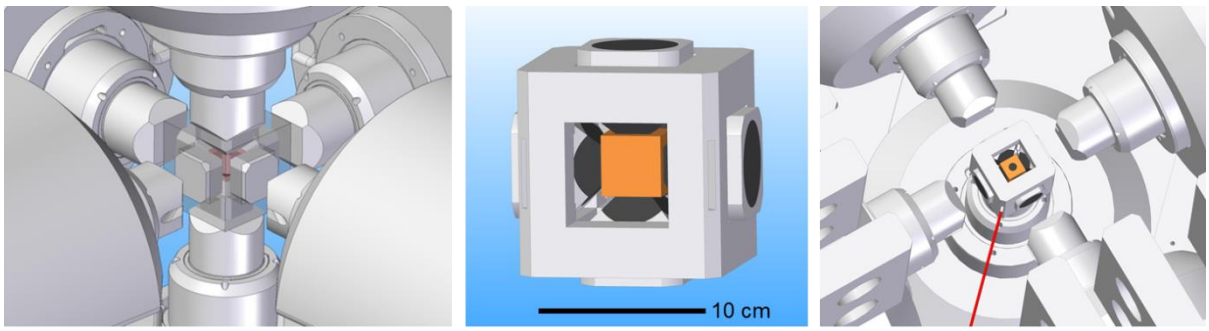

Fig. 3.5.11 3D views of the 6-6 cell assembly for the 6-rams-LVP in P61.2

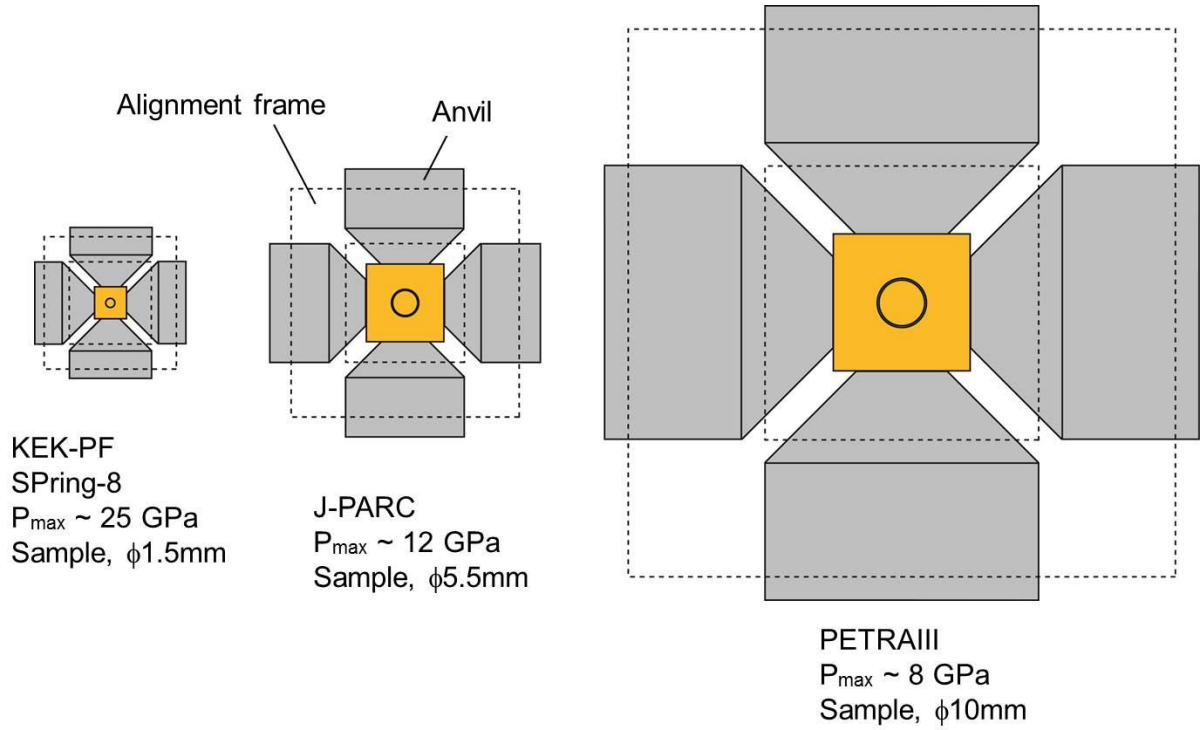

Fig. 3.5.12 Comparison of the 6-6 assembly of the P61.2 LVP to those at other facilities worldwide

3.6 Attenuation of X-rays by high-pressure cells

3.6.1 Overview

In case of in-situ X-ray observations using a LVP, the sample is surrounded by many materials: sample capsule; heater; thermal insulator; pressure transmitting medium; gasket. Most of them are made of ceramics, but sometimes even metals are used depending on experimental purposes. These materials in the X-ray beam path will attenuate the intensity both for the incident and diffracted beam. Fig. 3.6.1 shows a schematic illustration of role of high-pressure cell for X-ray attenuation.

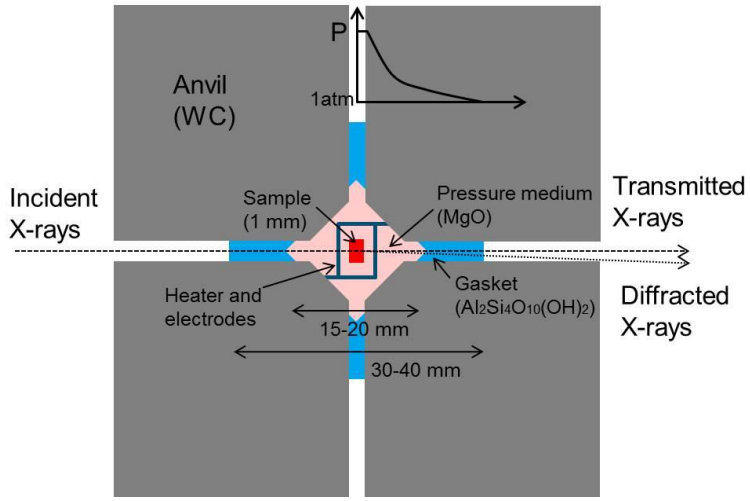

Fig 3.6.1
Schematic illustration of X-ray attenuation by various materials within a high-pressure cell

3.6.2 6-8 cell

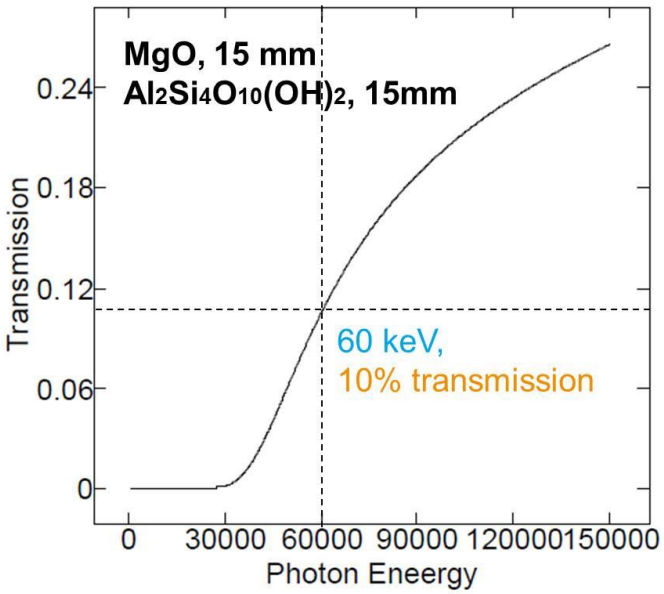

Fig 3.6.2
Transmission of X-rays as a function of photon energy through 15mm MgO and 15mm pyrophyllite

Fig. 3.6.2 shows the transmission of X-rays as a function of photon energy (eV) through 15mm MgO and 15 mm pyrophyllite, which are materials used for the pressure medium and the gasket. Photons with energies below 30 keV are almost completely attenuated by the surrounding materials and therefore cannot be used for X-ray diffraction and imaging experiments using a 6-8 assembly.

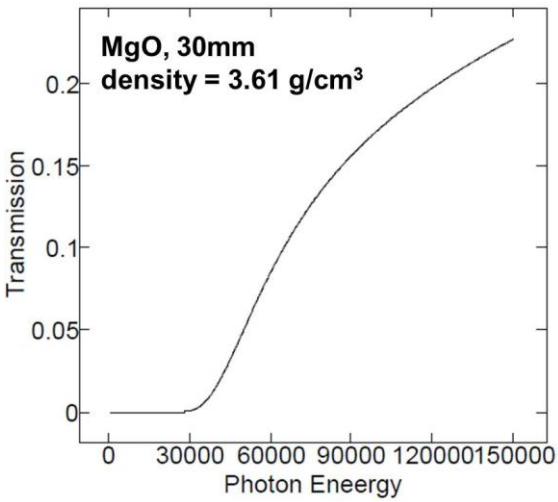

Fig 3.6.2
Transmission of X-rays through 30mm MgO

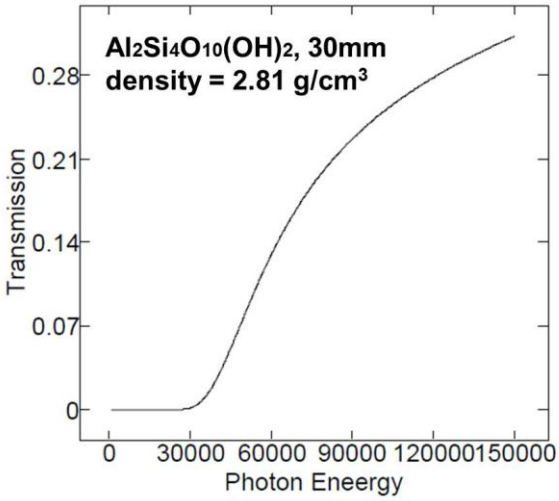

Fig 3.6.3
Transmission of X-rays through 30mm pyrophyllite

Fig. 3.6.2 and Fig. 3.6.3 show X-ray transmission of 30mm MgO and 30mm pyrophyllite separately. Attenuation of MgO is larger than that of pyrophyllite due to a high density of periclase (3.61 g/cm^3).

3.6.3 6-6 cell

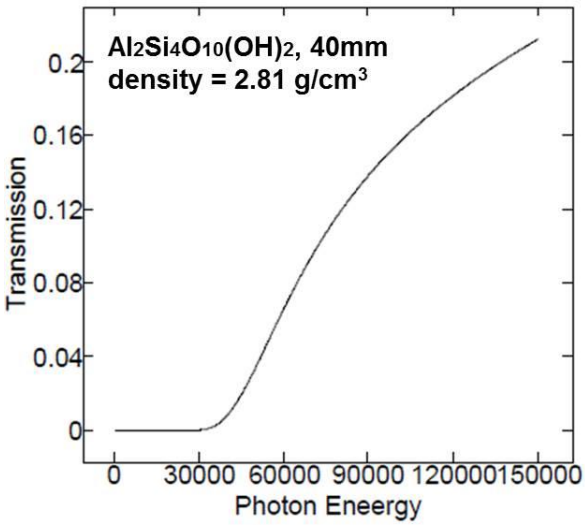

Fig 3.6.4
Transmission of X-rays as a function of photon energy through 40mm pyrophyllite

Fig. 3.6.4 shows transmission of X-rays as a function of photon energy through 40 mm pyrophyllite, which is close to the diagonal of pressure medium of a 6-6 cell assembly under high pressure. In this case, attenuation of X-rays is even larger than that of a 6-8 cell assembly because of the large distance (40 mm). The use of

alternative low-attenuation materials along the X-ray beam path should be investigated.

3.7 Ex-situ LVP instrument

A LVP instrument dedicated to ex-situ studies has been under operation since May 2013. This LVP is a 1000-ton press with a Walker module (mavo press LPR 1000-400/50, Max Voggenreiter GmbH) (Fig. 3.7.1). This instrument currently is manly used for DESY inhouse research, but it is considered to make it accessible also to external users in order to enhance collaborative research activities.

Fig 3.7.1
Second LVP instrument dedicated to ex-situ studies (mavo press LPR 1000-400/50).
In operation since May 2013

3.8 Pressure cells for user experiments

In order to attract users from many different research fields, standard cell assemblies that can be used by scientists who have no experience in performing high-pressure experiments using a LVP are necessary. Especially, in the European high-pressure community, the LVP technique is less popular than the DAC technique. It is therefore believed that reliable cell assemblies and supply of all necessary parts for user experiments are very important for the success of this beamline. After installation of the 6-rams-LVP, several standard cell assemblies will be developed both for the 6-8 and 6-6 systems. Then, to prepare the production of cell parts for user experiments, contacts to local machining companies will be initiated.

References

[1] Ito E, Katsura T, Yamazaki D, Yoneda A, Tado M, Nishihara E, Nakamura A, and Ochi T (2008) Manufacture of a new 6-axis apparatus. *The Review of High Pressure Science and Technology* **18**, 208-213.

[2] Wang Y, Durham WB, Getting IC, and Weidner DJ (2003) The deformation-DIA: a new apparatus for high temperature triaxial deformation to pressures up to 15 GPa. *Review of Scientific Instrument* **74**, 3002-3011.

[3] Yamazaki D, Ito E, Yoshino T, Tsujino N, Yoneda A, Guo X, Xu F, Higo Y, and Funakoshi K (2014) Over 1 Mbar generation in the Kawai-type multianvil apparatus and its application to compression of (Mg0.92Fe0.08)SiO3 perovskite and stishovite. *Physics of the Earth and Planetary Interiors* **228**, 262-267.

[4] Nishiyama N, Wang Y, Sanehira T, Irifune T, and Rivers ML (2008) Development of the multi-anvil assembly 6-6 for DIA and D-DIA type high-pressure apparatuses. *High Pressure Research* **28**, 307-314.

[5] Sano-Furukawa A, Hattori T, Arima H, Yamada A, Tabata S, Kondo M, Nakamura A, Kagi H, and Yagi T (2014) Six-axis multi-anvil press for high-pressure, high-temperature neutron diffraction experiments. *Review of Scientific Instrument* **85**, 113905.

4. Detector and detector mount

4.1 Overview

Using filtered white X-rays from the damping wigglers, energy dispersive X-ray diffraction measurements under high pressure and temperature will initially be performed with the 6-rams-LVP at P61.2. Two detector mounts for vertical and horizontal scans will be installed (Figs. 4.1.1 and 4.1.2). Using these detector mounts, two energy-resolved detectors (solid state detector) will be simultaneously used. This detector mount system enables performing time-resolved X-ray diffraction measurements and differential stress determination under high pressure and high temperature conditions.

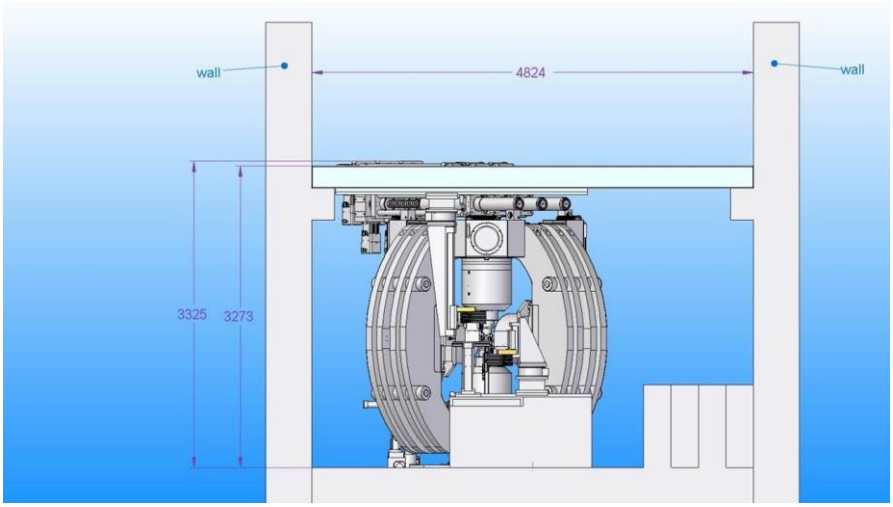

Fig. 4.1.1 Side view of the detector mounts

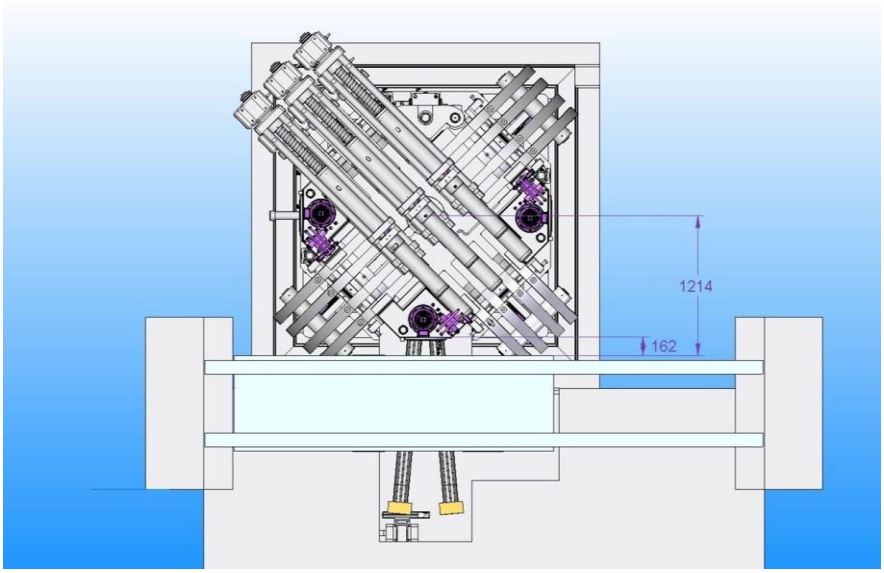

Fig. 4.1.2 Top view of the detector mounts

4.2 Detector mount

4.2.1 Collimator, slit, and detector unit

A collimator and a xy-slit will be used to block diffracted X-rays from the sample capsule, pressure medium, and gaskets (Fig. 4.2.1). Collimators with four different openings will be used depending on experimental purposes: 0.03 mm; 0.05 mm; 0.1 mm; 0.2 mm. The tip of the collimator to cut the X-rays is made of tungsten carbide.

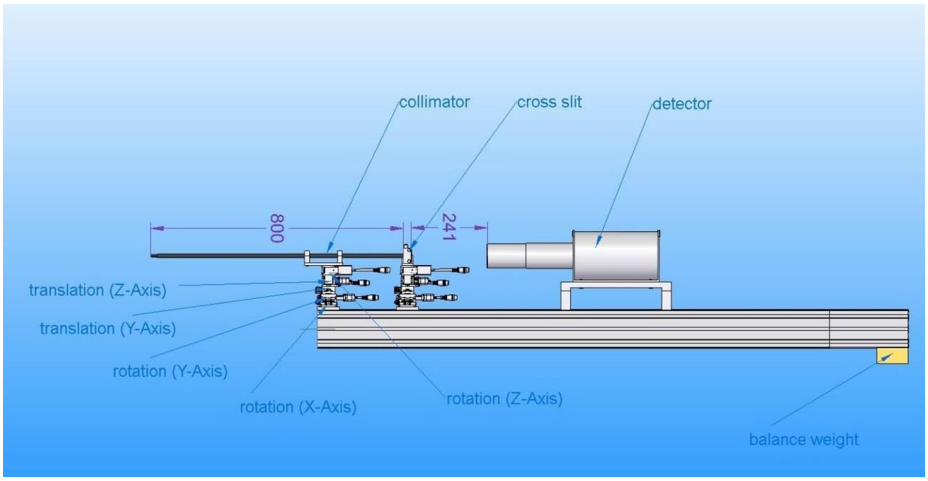

Fig. 4.2.1 View of collimator, slit, and detector unit

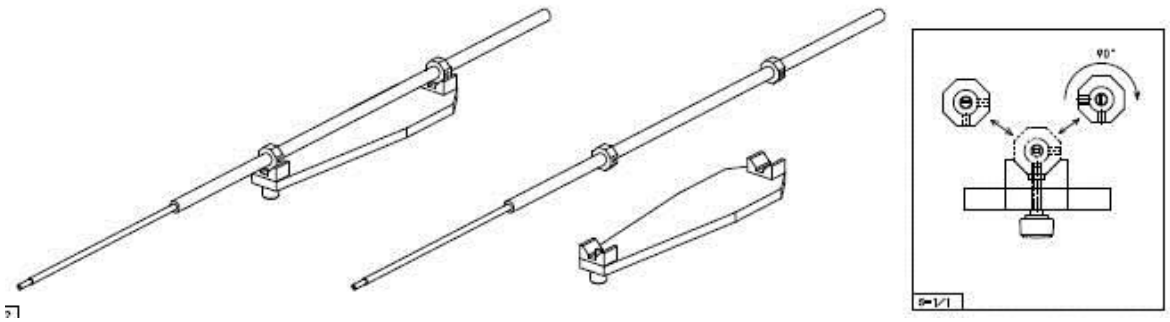

Fig. 4.2.2 Collimator unit (exchangeable and rotatable)

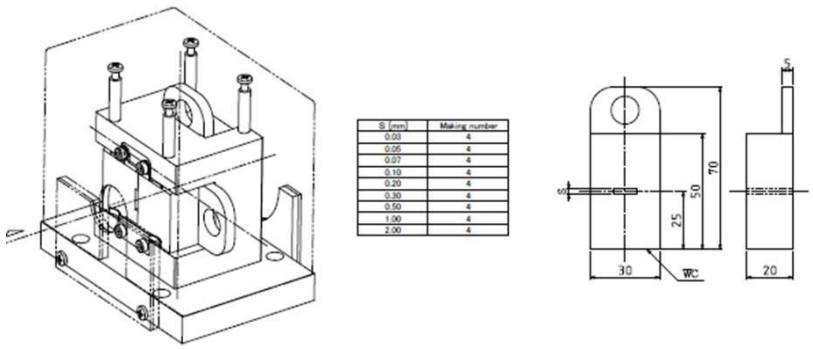

Fig. 4.2.3 Receiving slit box with a pair of tungsten carbide slits

As shown in Fig. 4.2.2, collimators are exchangeable and 90 degrees rotatable. The length of the collimator is 800 mm. The distance between the sample in the 6-rams-LVP and the entrance of the collimator is about 200 mm. Fig. 4.2.3 shows a receiving slit box with a pair of tungsten carbide slits. Thickness of a WC slit is 20 mm. Nine slits with different openings (mm) will be prepared:

0.03	0.05	0.06	0.1	0.2	0.3	0.5	1.0	2.0

A collimator unit and a receiving slit box are located on a 5-axis alignment system allowing to align a collimator and a pair of slits to maximize the diffracted signals:

- ϕ-x (±4.5 degrees)
- ϕ-y (±4.5 degrees)
- ϕ-z (±4.5 degrees)
- y-translation (±5 mm)
- z-translation (±2.5 mm).

4.2.2 Vertical

Figure 4.2.4 shows the vertical detector mount. There are five movements: ϕy rotation (vertical), -1 to +25°: ϕz rotation (horizontal), ±10°; x-translation, y-translation, z-translation. Travel lengths for xyz translations depend on the design of the detector mount.

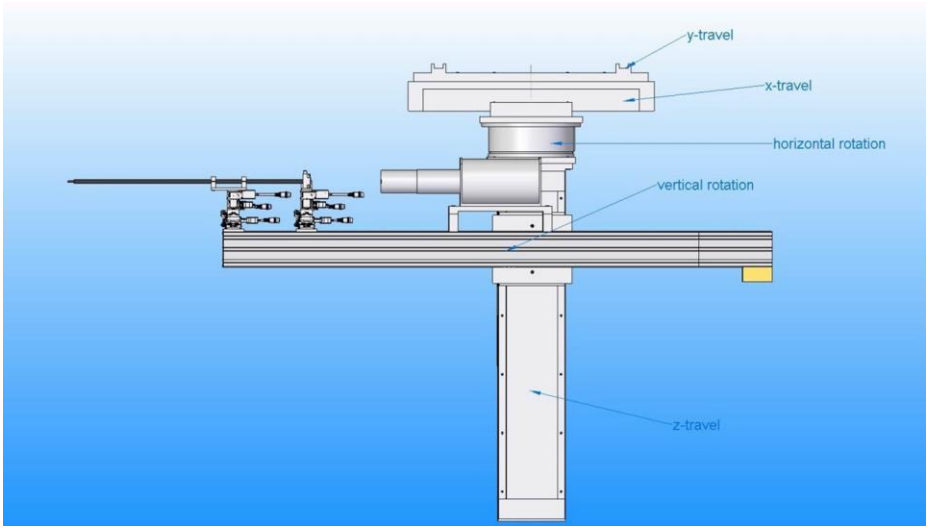

Fig. 4.2.4 **V**ertical detector mount

4.2.3 Horizontal

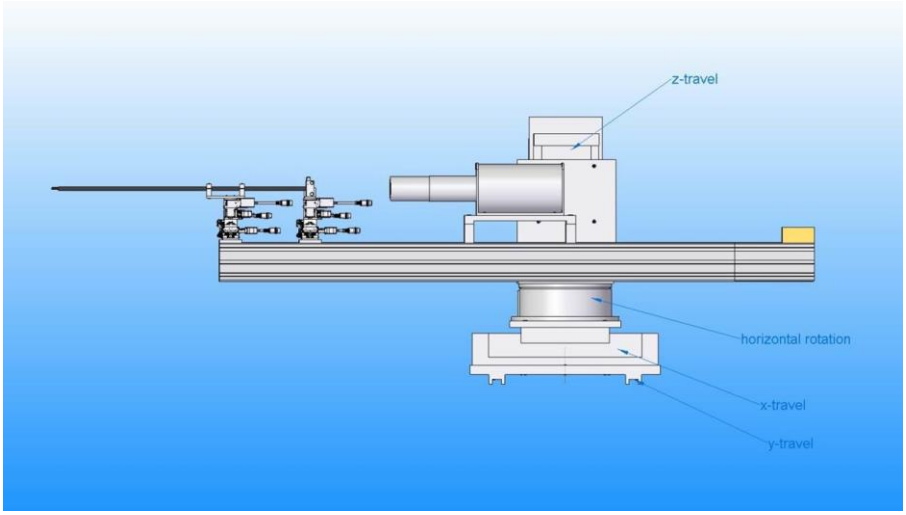

Fig. 4.2.5 The horizontal detector mount

Figure 4.2.5 shows the horizontal detector mount. There are four movements: ϕz rotation (horizontal, ±10°); x-translation; y-translation; z-translation. Travel lengths for xyz translations depend on the design of the detector mount.

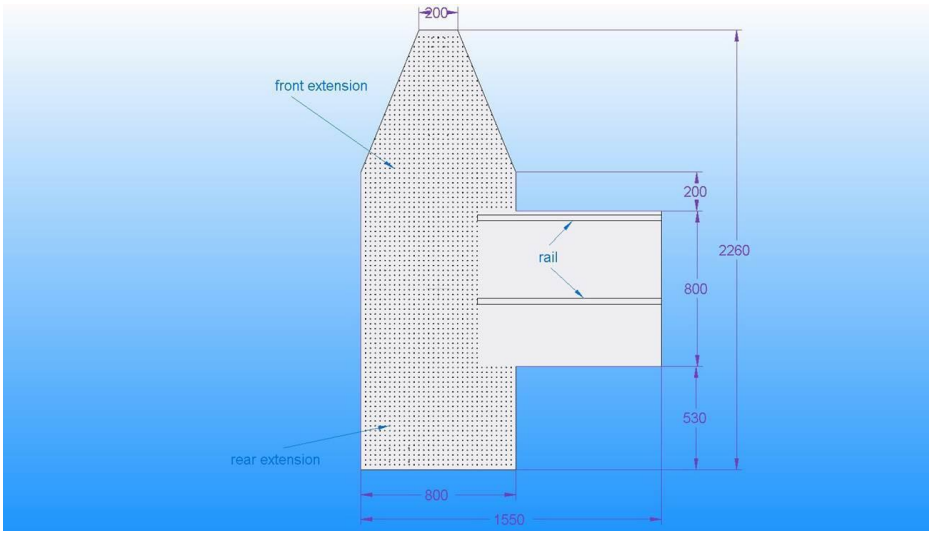

Fig. 4.2.6 Table for the horizontal detector

Fig. 4.2.6 shows a table for the horizontal detector-mount. Two rails for y-translation are fixed on this table. On the front extension of this table, a direct beam stopper will be located. On the rear extension, a radiographic imaging system will be located. The position of the imaging system is not fixed. It is possible to locate the imaging system on the front extension for better imaging. This table for the horizontal detector-mount is removable. Then, other tables for different experimental purposes can be attached.

4.2.4 Direct beam stopper

A direct beam stopper unit will be located on the front extension of the horizontal detector-mount table. It can be moved up and down, where the up-position is for X-ray diffraction measurements and the down-position is for imaging.

4.2.5 Radiographic imaging

A radiographic imaging system will be located on the rear extension of the horizontal detector-mount table. This imaging system consists of a YAG phosphor, a mirror, an objective lens and a CCD camera. The YAG phosphor converts X-ray contrast into that of visible light. Then, a microscope system with a CCD camera is used to observe the sample under high-pressure and temperature. An additional filter system will be used for the radiographic imaging because the beam size is much larger than that for X-ray diffraction measurements.

4.3 Detector

4.3.1 Pure Ge detector

For the energy dispersive X-ray diffraction measurements, energy resolving detectors with sufficient efficiency are needed. Pure Ge detectors are being widely used at other LVP beamlines and will also be the first choice for P61.2. A Ge-detector manufactured by CANBERRA, Low Energy Germanium Detector (LEGe), seems to be appropriate for the planned experiments at this beamline. Fig. 4.3.1 shows the efficiency of this detector as a function of photon energy which is in the range 2-7% for photon energies of 20-100 keV [1].

Fig. 4.3.2 shows a series of LEGs offered by CANBERRA. For P61.2, it is planned to choose model GL0110 which is also being used at LVP beamline BL04B1 in SPring-8.

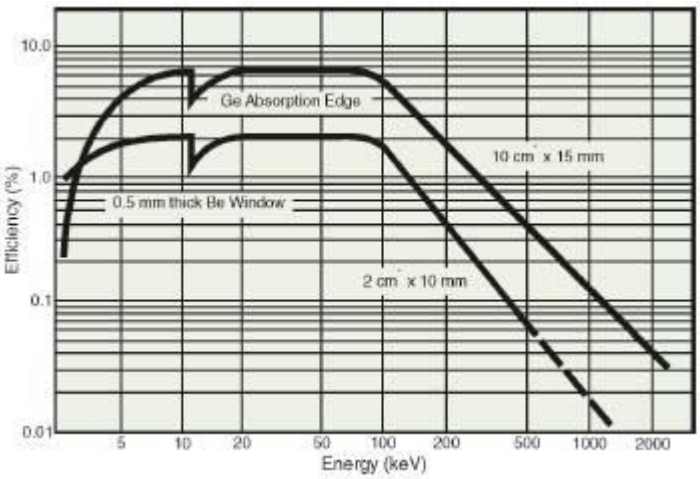

Fig 4.3.1
Efficiency of a LEGe (CANBERRA) detector as a function of photon energy [1]

GENERAL SPECIFICATIONS AND INFORMATION

Model Number	Area (mm^2)	Thickness (mm)	Be Window Thickness mm (mils)	Resolution (eV FWHM)** (at optimum settings)		Preamplifier Type
				5.9 keV	122 keV	
GL0055	50	5	0.025 (1)	145	500	I-TRP
GL0110	100	10	0.025 (1)	160	500	I-TRP
GL0210	200	10	0.15 (5)	195* (170)	520	RC*
GL0510	500	10	0.15 (5)	250	550	RC
GL0515	500	15	0.15 (5)	250	550	RC
GL1010	1000	10	0.5 (10)	300	620	RC
GL1015	1000	15	0.5 (10)	300	620	RC
GL2020	2000	20	0.5 (20)	400	680	RC

Fig 4.3.2
A series of LEGs [1]. GL0110 is the first choice for P61.2

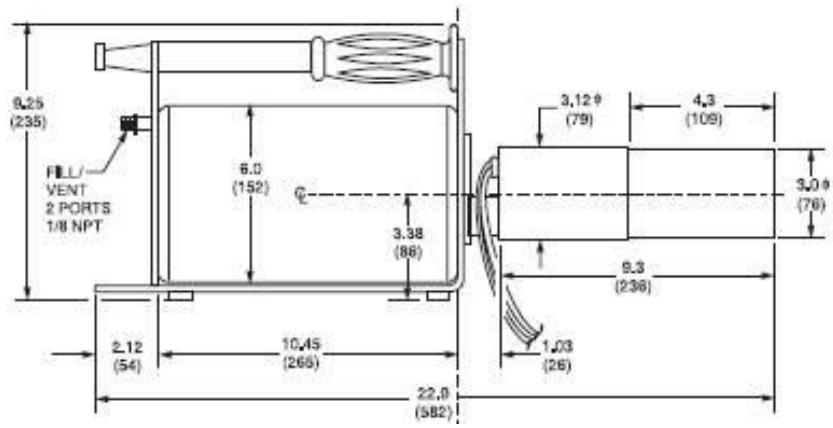

Fig 4.3.3
Dimensions of a LEGe with MAC-two day [1]

Fig. 4.3.3 shows dimensions of a LEGe with a small cryostat (MAC-two day). Its specifications are: empty weight: 5.1 kg; full weight: 7.1 kg; LN2 capacity: 2.5 liters, holding time: 2 days; cooling down time: 2 hrs. Since two detectors will be used simultaneously in P61.2, a small cryostat is essential in order to avoid collisions with the other detector.

4.3.2 CdTe detector

Recently, CdTe solid state detectors (Fig. 4.3.4) have become commercially available [2] and have been used at synchrotron facilities (e.g., BL04B2, SPring-8 [3]). Fig. 4.3.5 shows the efficiency of a CdTe detector as a function of photon energy. The efficiency is practically 100% between 10 and 50 keV and still exceeds 50% even at 100 keV. It is therefore much higher than that of a Ge detector.

Fig 4.3.4
CdTe solid state detector XR-100T-CdTe (Amptek) [2]

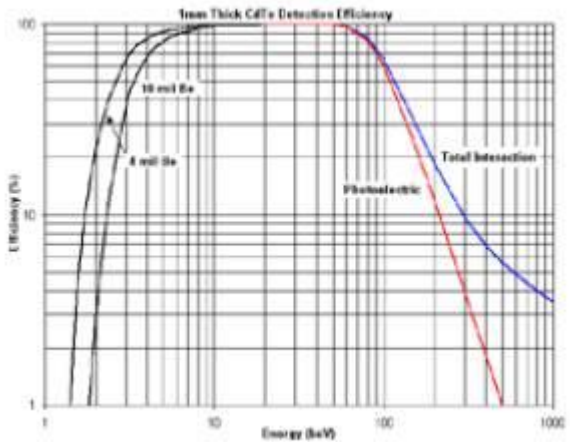

Fig 4.3.5 Detector efficiency as a function of photon energy [2]

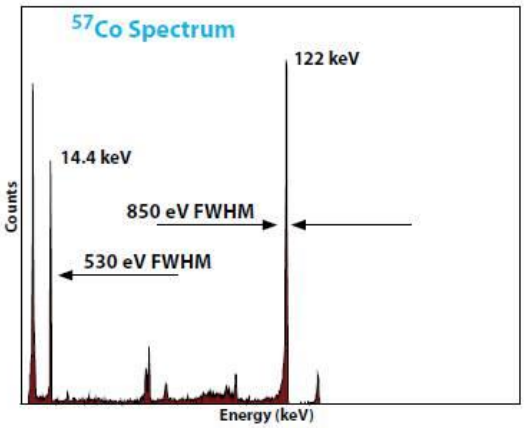

Fig 4.3.6 Example spectrum of Co [2]

Fig. 4.3.6 shows an example spectrum obtained using a CdTe detector (XR-100T-CdTe, Amptek). The FWHM of the ^{57}Co peak (122 keV) is 850 eV, which is about 1.6 times broader than that obtained by a Ge detector (LEGe, CANBERRA, 500 eV). The biggest advantage of a CdTe detector is its small size because a cryostat for LN_2 cooling is not needed. To our knowledge, a CdTe detector has not yet been employed at LVP beamlines in synchrotron facilities. Currently, we are exploring the possibility of performing test experiments at SPring-8 with a CdTe detector for XRD measurements under high pressure and temperature using a LVP instrument. The tests could e.g. be done at BL04B1 (SPring-8), a possible beamtime could be already in fall / winter 2015.

4.4 Time-resolved energy dispersive X-ray diffraction measurements

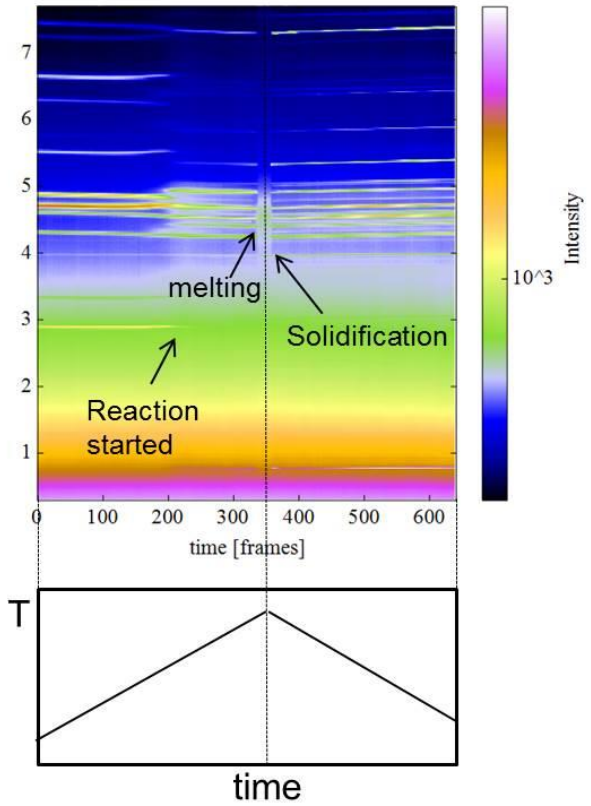

Fig 4.4.1
An example of time-resolved XRD studies carried out PETRA III beamline P02.1 at 1-bar and high temperatures

Fig. 4.4.1 shows results of time-resolved XRD studies carried out at PETRA III beamline P02.1 (powder XRD) at 1-bar and high temperature. Data collection was performed every 10 seconds. The temperature was increased at a certain rate (e.g., +10 K/min) and at the maximum temperature, a cooling process at the same rate (e.g., -10 K/min) started. In the 2D image (2Θ vs. time, intensity is shown as the color contour), the reaction of the sample under high temperature is readily seen. We can also observe melting of the sample and – in the molten state - diffused scattering from the sample is observed. The time-resolved technique is a very powerful tool to observe reaction processes. Using the obtained data, the mechanism of formation of materials and textures can be discussed.

Using the energy-dispersive setup combined with the 6-rams-LVP, time-resolved XRD studies under high pressure and temperature can be performed. Fig. 4.4.2 shows a detector setup for time-resolved X-ray diffraction measurements. Two detectors are located at identical positions (e.g., +6° and -6°), doubling the count rate of diffracted signals.

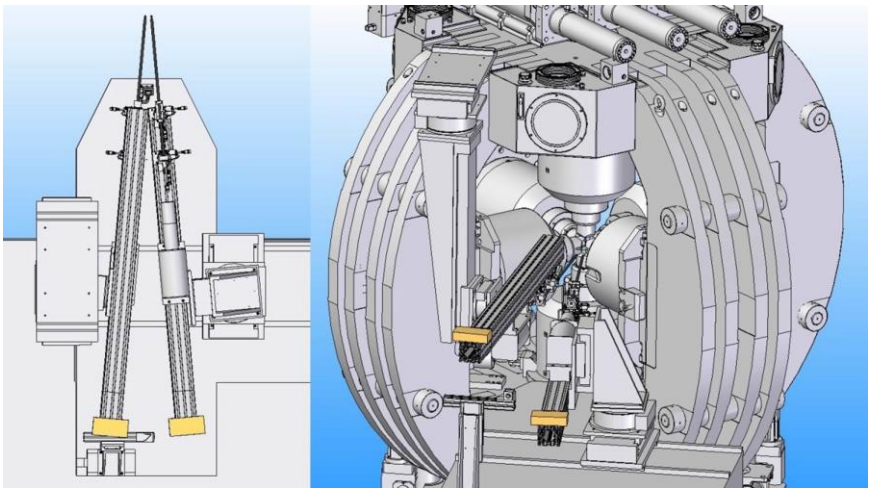

Fig. 4.4.2 Detector setup for time-resolved X-ray diffraction measurements

There are two main research targets using this technique:

- observation of formation processes of high-pressure phases
- brittle fracture and deformation of materials under high pressure

We believe that there are many possible research projects using this experimental set-up for time-resolved XRD measurements under high pressure and temperature both for Earth science and materials science.

4.5 Stress analysis under high pressure and temperature

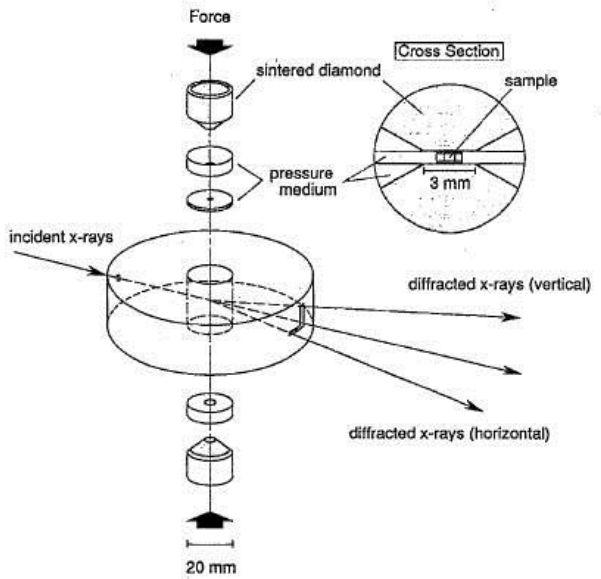

Fig 4.5.1
X-ray diffraction geometry for stress analysis using a Drickamer-type apparatus [4]

Fig. 4.5.1 shows the X-ray diffraction geometry for stress analysis using a Drickamer-type apparatus [3]. Funamori *et al.* used two Ge solid state detectors at the horizontal and the vertical positions to determine differential stress under pressure.

Using the detector mount system in P61.2, we can perform the same measurements using the 6-rams-LVP.

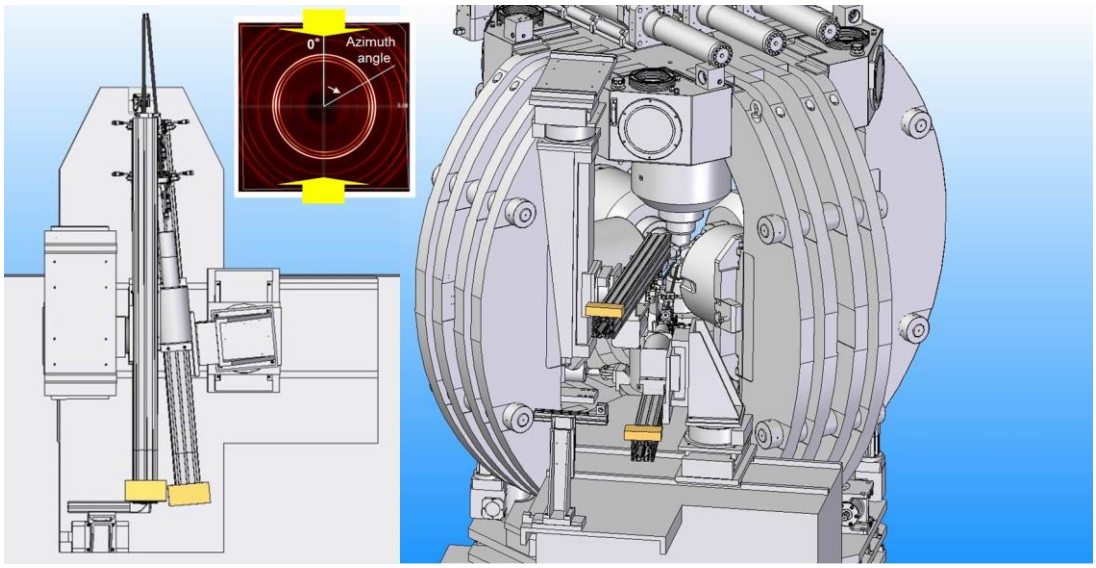

Fig. 4.5.2 Detector setup for differential stress measurements

Fig. 4.5.2 shows the detector setup for differential stress measurements using the 6-rams-LVP. The vertical and horizontal detectors are fixed at the same diffracted 2Θ angle. A radiographic imaging system is located at the rear extension of the detector table. We can observe stress-strain curves of materials under high pressure and temperature using this setup. The use of the large 6-6 assembly enables performing measurements for natural rock samples with a diameter > 5 mm.

4.6 Liquid structure analysis using the 6-6 configuration

Since the 6-rams-LVP has wide openings in the vertical direction, X-ray diffraction measurements to determine liquid structure can be carried out using the 6-6 configuration. Fig. 4.6.1 shows a detector setup for this study. A large 6-6 cell assembly allows collecting data without contamination of peaks from the surrounding cell materials.

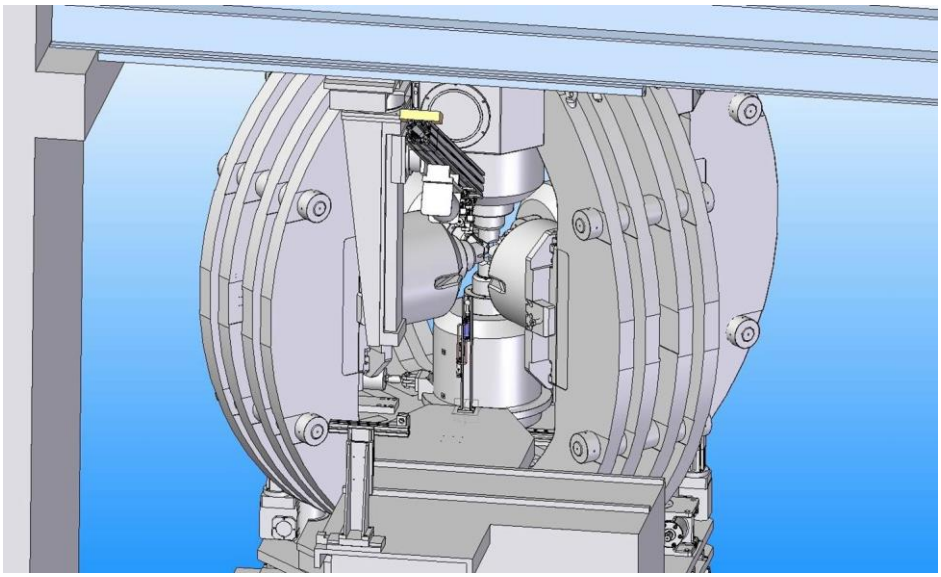

Fig. 4.6.1 Detector setup for liquid structure analysis

References

[1] http://www.canberra.com/products/detectors/germanium-detectors.asp

[2] http://www.amptek.com/products/xr-100t-cdte-x-ray-and-gamma-ray-detector/

[3] Kohara S, BL04B2: High energy X-ray diffraction beamline, *in SPring-8 Annual Report in 2012.*

[4] Funamori N, Yagi T, and Uchida T (1994) Deviatoric stress measurement under uniaxial compression by a powder x-ray diffraction. Journal of Applied Physics 75, 4327-4331.

5. Future developments

5.1 High energy monochromatic X-ray capability

5.1.1 Overview

The main technique at P61.2 will be time-resolved energy dispersive X-ray diffraction measurements under high pressure and temperature using a 6-rams-LVP. It is planned to start “friendly user” operation in summer 2017. As a future development (2018-2020), it is planned to install a monochromator in the optics hutch in order to add experimental capabilities using monochromatized X-rays. The following requirements for a monochromator in P61.2 are considered:

- monochromatic energy range from 60 to 120 keV.
- $\Delta E/E$ ~ 10^(-3)
- compact design (2m x 2m for footprint)
- small and horizontal beam-offset (<10 mm)
- suitable (LN_2 ?) cooling of the first crystal because of the high-heat load of the filtered damping wigglers beam.

5.1.2 Monochromator

Fig 5.1.1
A photo of a double Laue-crystal monochromator (idt)

A possible solution to fulfill all the requirements could be a compact double Laue-crystal monochromator. Fig. 5.1.1 shows an example of this type of monochromator manufactured by idt [1], which has been installed in other beamlines using high-energy X-rays (e.g. P07 at PETRA III) and will also be constructed for the new PETRA III extension beamline P21. After starting user operation of P61.2 for time-resolved EDXRD measurements, possible science targets of studies using monochromatic X-rays with the 6-rams-LVP will be discussed with the user community.

5.1.3 Large radius Debye-Scherrer camera

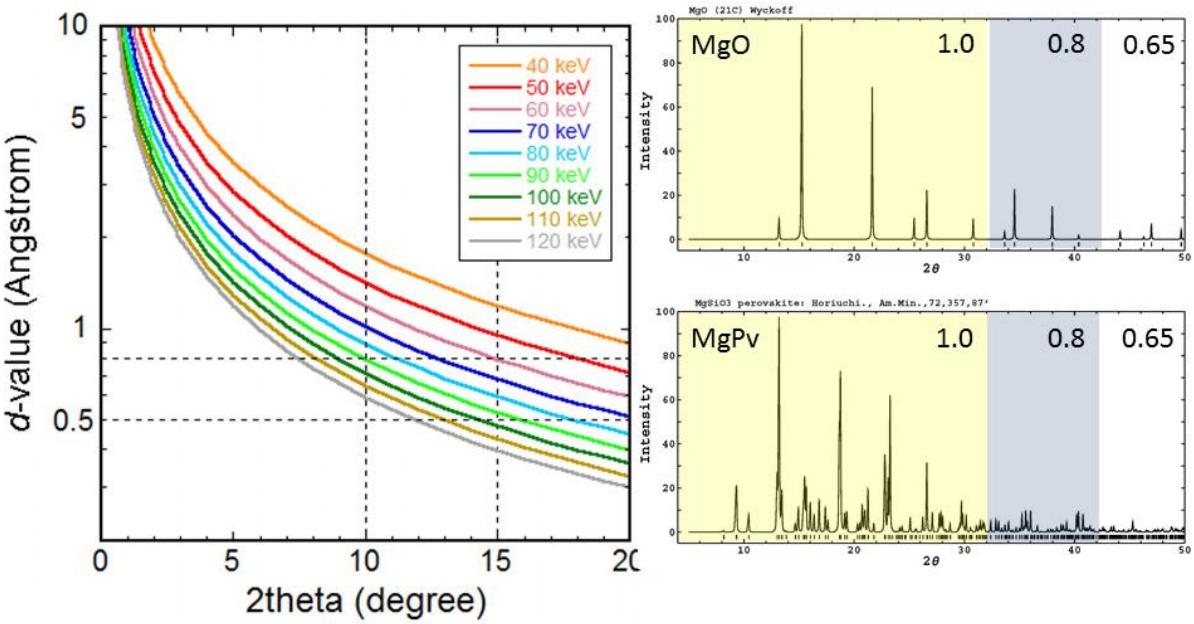

Fig. 5.1.2 *d*-value ranges that can be observed using monochromatic X-rays with different photon energies. E > 80 keV is preferable.

Fig. 5.1.2 shows *d*-value ranges that can be observed using monochromatic X-rays with different photon energies. XRD patterns of MgO and $MgSiO_3$-perovskite (MgPv) are also shown. In order to refine atomic positions using a powder XRD profile, a wide *d*-value range should be covered. However, in case of XRD measurements using a LVP instrument, the observable maximum diffracted angle is limited to about 10° for the 6-8 configuration resp. 25° for the 6-6 configuration. For the 6-8 configuration, X-rays with E = 100 – 120 keV are preferable, resp. E = 60 – 80 keV for the 6-6 configuration.

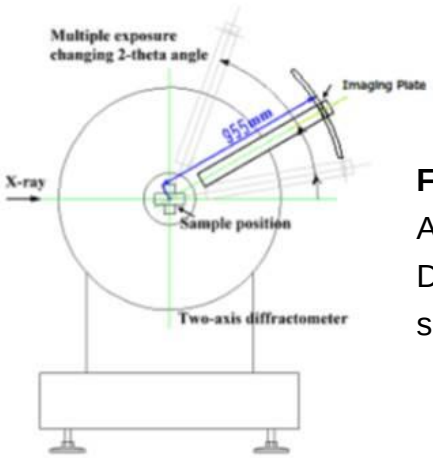

Fig 5.1.3
A large radius Debye-Scherrer camera set-up in SPring-8 [2]

Fig. 5.1.3 shows a large radius Debye-Scherrer camera setup at BL15XU (SPring-8) [2]. This is a simple and high throughput setup which may also be a good option for the 6-rams-LVP in P61.2.

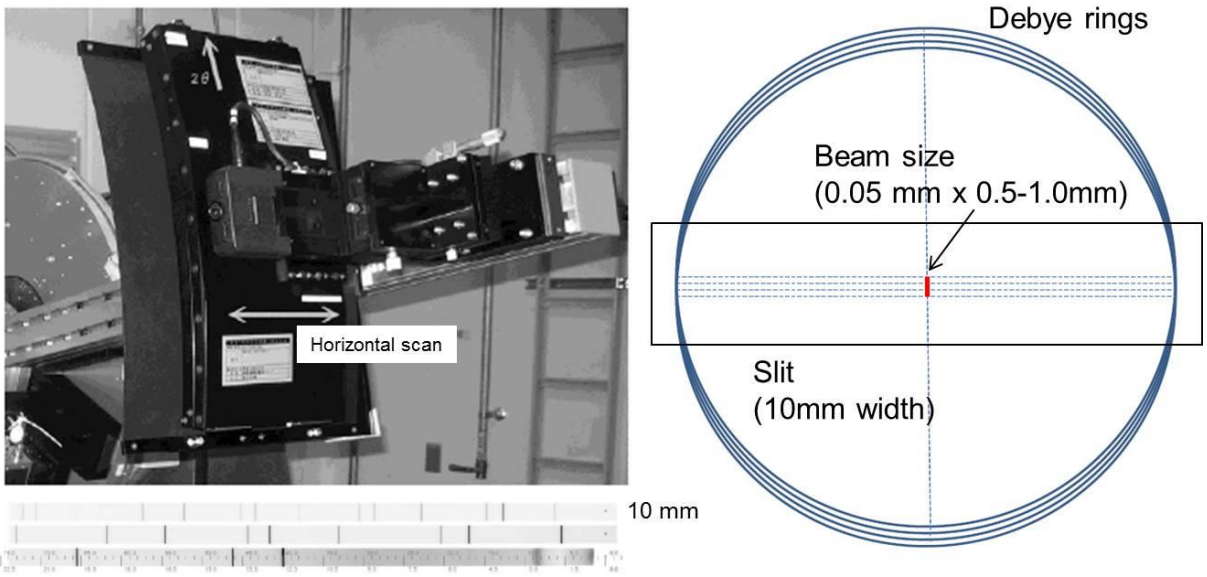

Fig. 5.1.4 Image plate detector system of large radius Debye-Scherrer camera.

Fig. 5.1.4 shows an image plate detector system making a large radius Debye-Scherrer camera [2]. There is a slit with 10 mm opening to record a strip of Debye-rings. The imaging plate can be moved horizontally to record several strips on an imaging plate. The imaging plate should be read using a separate offline reader.

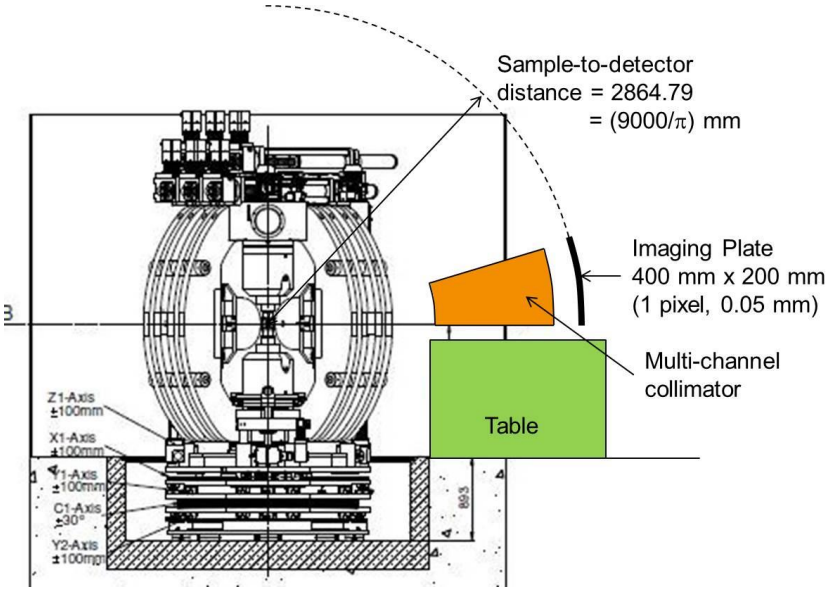

Fig 5.1.5
A conceptual design of a large radius Debye-Scherrer set-up for 6-rams-LVP

Fig. 5.1.5 shows a conceptual design of a large radius Debye-Scherrer setup for the 6-rams-LVP in P61.2. Parameters of this setup:

- Sample to detector distance — 2864.79 (= 9000/π) mm.
- Detector size — 400 mm x 200 mm
- X-ray range — 60-120 keV
- 2Θ coverage — 8° (=400/9000*180)
- 2Θ range — max. 10° for 6-8 cell (1-2 shots)
  max. 25° for 6-6 cell (3-4 shots)
- Pixel size — 0.05 mm x 0.05 mm
- 2Θ-pixel ratio — 1 pixel = 0.001° (=0.05/400*8)

As the sample in high-pressure cell is surrounded by many materials, a device to collimate diffracted X-rays is needed in order to eliminate signals from the surrounding materials. A multi-channel collimator [3] is an appropriate device for this setup. The multi-channel collimator is oscillated during data collection. Since the 6-rams-LVP has wide openings in the vertical directions, the large Debye-Scherrer setup is suitable for the 6-6 configuration.

5.1.4 Spiral slit

High-energy monochromatic X-rays have been employed for stress analysis under high pressure and temperature [4]. In most cases, a collimation device is not used [5]. Therefore, the obtained X-ray diffraction patterns contain unnecessary peaks from the surrounding materials such as heater, pressure medium, and gaskets.

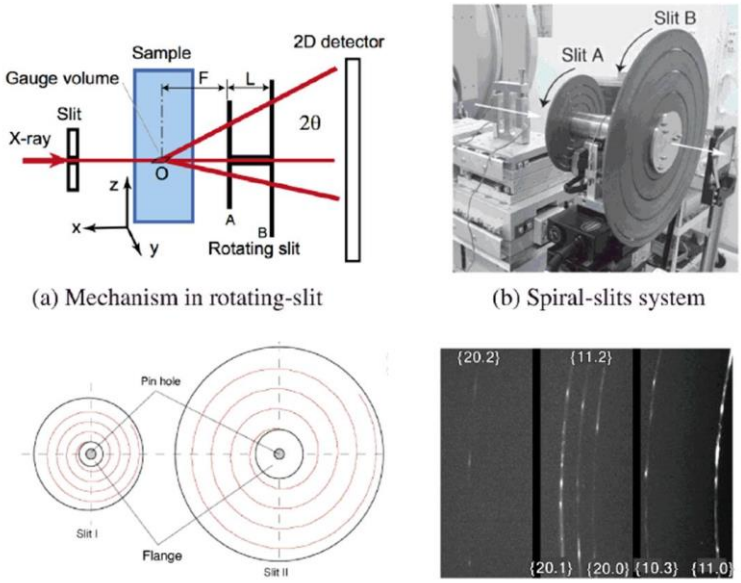

Fig. 5.1.6 Spiral slit system at BL22XU, SPring-8 [6, 7]

Fig. 5.1.6 shows a spiral slit system developed at BL22XU, SPring-8 [6, 7]. In this beamline, the spiral-slit system has been used to measure internal stresses in structural materials such as magnesium alloys. Its concept can also be used for stress analysis under high pressure and temperature generated in a LVP instrument. Development of a spiral-slit system dedicated to a combination of high-energy monochromatic X-rays (60-120 keV) and the 6-rams-LVP is required.

5.2 Multi-element SSD for stress analysis

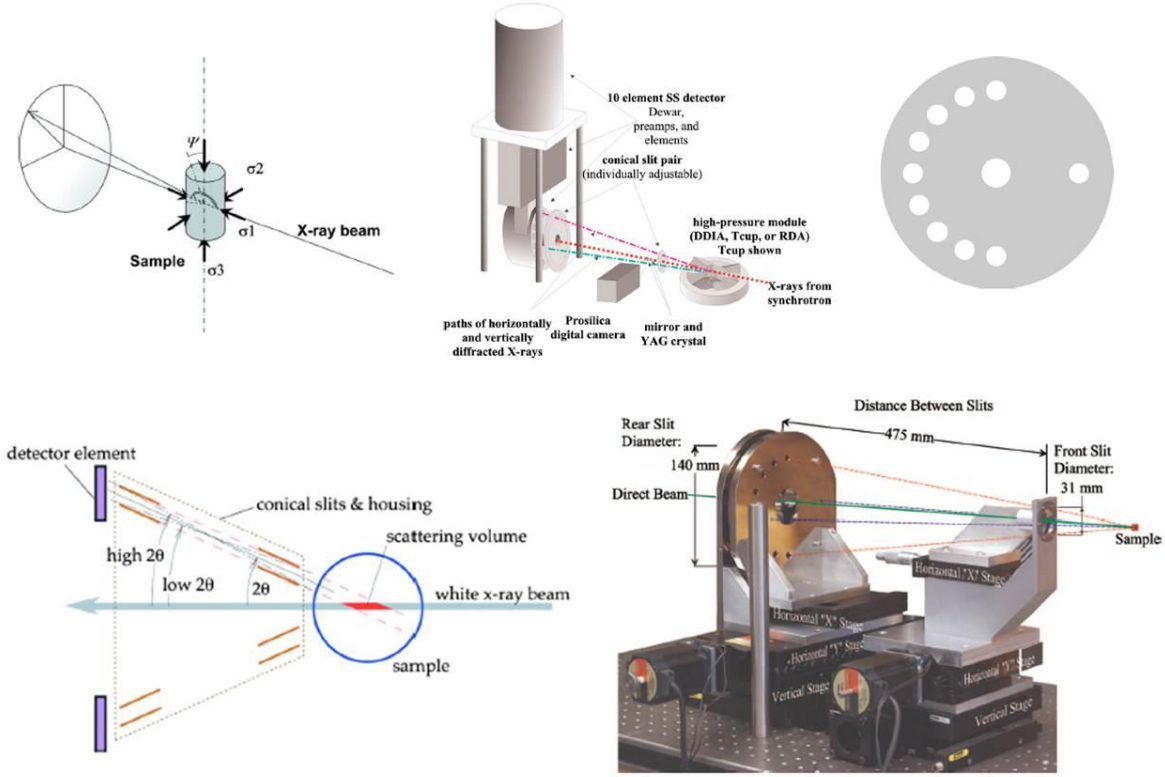

Fig. 5.2.1 A setup using a multielement energy dispersive detector for stress analysis under high pressure and temperature

Using the detector mount system for P61.2, stress analysis can be performed using two SSD detectors at two different positions: Ψ = 0° and 90°. We can calculate differential stress by assuming cylindrical symmetry of the stress field. In order to determine the differential stress more precisely, the number of detectors can be increased using a multielement energy dispersive detector [8]. Fig. 5.2.1 shows an example of the setup at NSLS. In future, we may install a similar set-up in P61.2. A disadvantage of this setup, however, is that a diffracted angle is fixed to a certain value (6.5° in NSLS).

5.3 Time-resolved high temperature XRD under 1 bar

TZF 15/610

Technical data

Model	Max temp (°C)	Heat-up time (mins)	Dimensions: Max outer diameter accessory tube (mm)	Dimensions: Heated length (mm)	Tube length for use in air (mm)	Tube length for use with modified atmosphere (mm)	Dimensions: External H x W x D (mm)	Max power (W)	Holding power (W)	Thermocouple type	Weight (kg)	Power supply		
												Volt	Phase	Ampere per phase
TZF 15/610	1500	75	90	610	1200	1500	650 x 1080 x 430	8000	4000	R	70	200-240 380-415 220-240	single phase 3 phase + N 3 phase delta	60 22 38
TZF 16/610	1600	-	90	610	1200	1500	650 x 1080 x 430	9150	4500	R	74	220-240 380-415 220-240	single phase 3 phase + N 3 phase delta	62 25 40
TZF 17/600	1700	150	90	600	1200	1500	880 x 1020 x 630	6800	3800	B	280	220-240 208 380-415 220-240	single phase single phase 3 phase + N 3 phase delta	46 48 28 34
TZF 18/600	1800	150	90	600	1200	1500	945 x 1020 x 630	5700	-	Pt20%Rh/Pt40%Rh	280	220-240 380-415 220-240 208	single phase 3 phase + N 3 phase delta 3 phase delta	40 24 28 30

Fig. 5.3.1 A tube furnace that can be used for XRD measurements at 1 bar and high-temperature up to 1800°C

The high intensity of the filtered white beam from the damping wigglers is also beneficial for time-resolved high-temperature XRD measurements under 1 bar. Fig. 5.3.1 shows a tube furnace with maximum temperature of 1800°C. Since the opening of the tube is small, high energy X-rays are preferred for XRD measurements using this instrument.

The bottom piston and hydraulic ram is movable in order to make space in the 6-rams-LVP. Then, a table for a high-temperature furnace can be installed. Stages for xyz translations for the 6-rams-LVP can be used to align the sample in the tube furnace to the gauge volume of XRD measurements.

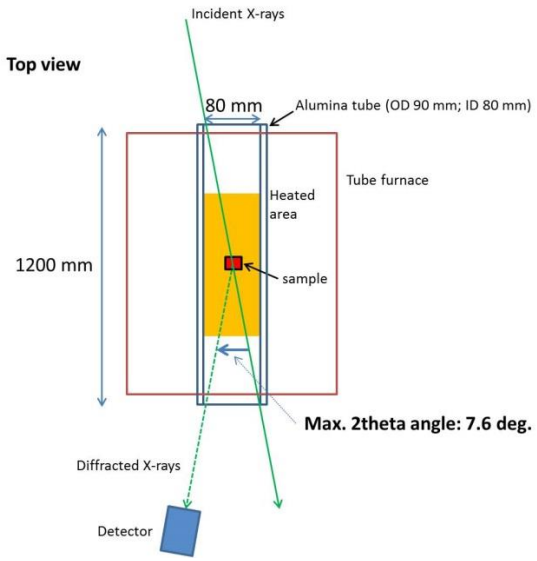

Fig 5.3.2
A conceptual illustration of high-temperature XRD measurements using a tube furnace in P61.2

Fig. 5.3.2 shows a conceptual illustration of high-temperature XRD measurements using a tube furnace in P61.2. This setup enables carrying out time-resolved XRD measurements up to 1800°C.

References

[1] http://www.idtnet.co.uk/double_laue_mono.html

[2] Tanaka M, Katsuya Y, and Yamamoto A (2008) A new large radius imaging plate camera for high-resolution and high-throughput synchrotron x-ray powder diffraction by multiexposure method. *Review of Scientific Instruments* **79**, 075106.

[3] Yaoita K, Katayama Y, Tsuji K, Kikegawa T, and Shimomura O (1997) Angle-dispersive diffraction measurement system for high-pressure experiments using a multichannel collimator. *Review of Scientific Instruments* **68**, 2106-2110.

[4] Uchida T, Wang Y, Rivers ML, and Sutton SR (2004) Yield strength and strain hardening of MgO up to 8 GPa measured in the deformation-DIA with monochromatic X-ray diffraction. *Earth and Planetary Science Letters* ***226***, 117-126.

[5] Wang Y, Rivers M, Sutton S, Nishiyama N, Uchida T, and Sanehira T (2009) The large-volume high-pressure facility at GSECARS: a “Swiss-army-knife” approach to synchrotron-based experimental studies. *Physics of the Earth and Planetary Interiors* **174**, 270-281.

[6] Suzuki K, Shobu T, Shiro A, and Toyokawa H (2014) Evaluation of internal stresses using rotating-slit and 2D detector. *Materials Science Forum* **772**, 15-19.

[7] Suzuki K, Shobu T, Shiro A, and Zhang S (2014) Internal stress measurement of weld part using diffraction spot trace method. *Materials Science Forum* **777**, 155-160.

[8] Weidner DJ, Vaughan MT, Wang L, Long H, Li L, Dixan NA, and Durham WB (2010) Precise stress measurements with white synchrotron x rays. *Review of Scientific Instruments* **81**, 013903.

Timeline

Oct. 2010	1st user workshop in Lüneburg
Sep. 2012	2nd user workshop at DESY, Hamburg
Apr. 2015	completion of hall civil engineering and pit for LVP
Jun. 5th 2015	TDR review
Jul. 2015	installation of 6-rams LVP
1Q 2016	installation of concrete shielding hutches
2Q 2016	3rd user workshop
3Q 2016	installation of detector mount
4Q 2016	installation of beamline optical components
1Q 2017	storage ring modification & front end installation
2Q 2017	commissioning of EDXRD under high-PT
Summer 2017	first user experiments for EDXRD
2018-2019	Monochromator installation
2019-	User operation both for EDXRD and ADXRD